# Predicting Absolute and Site Specific Acidities for Zeolite Catalysts by a Combined Quantum Mechanics/Interatomic Potential Function Approach†

**Uwe Eichler, Martin Brändle, and Joachim Sauer***

*Max-Planck-Gesellschaft, Arbeitsgruppe Quantenchemie an der Humboldt-Universität, Jägerstrasse 10/11, D-10117 Berlin, Germany*

*Received: June 2, 1997; In Final Form: August 28, 1997*⊗

The approach used describes the Brønsted site by the Hartree−Fock method and a T(O)DZP basis set, while the periodic zeolite framework and the interaction between the active site and the framework are described by a shell model potential parametrized on the same type of ab initio data for cluster models. It is capable of reproducing the effect of the crystallographic position and of different framework structures on the properties and reactivity of zeolitic Brønsted sites. For H-faujasite (Si/Al = 47) protonation of all four crystallographically different oxygen positons is considered. In agreement with experiment protonation on O(1) and O(3) is preferred. For the orthorhombic form of H-ZSM-5 (Si/Al = 95) protonation of the Al(7)−O(17)H−Si(4) site proves more stable than protonation at the Al(12)−O(24)−Si(12) site located at the channel intersection. In agreement with experiments, the OH vibrational frequency is predicted to decrease according to O(1)H-FAU > H-ZSM-5 > O(3)H-FAU, and the $^1$H NMR chemical shift to increase in the same sequence. The method also yields absolute and site specific acidity values. The deprotonation energy—a measure of acidity—obtained by this combined scheme is decomposed into the quantum mechanical contribution for the cluster itself and the long-range contribution. The former reflects the structural constraints imposed on the active site by the framework and the latter the influence of the crystal potential. With increasing cluster size the long-range correction decreases slowly, while the total energy stays remarkably stable within a few kJ/mol. For H-ZSM-5 and H-faujasite heats of deprotonation (proton affinities) of 1205 and 1169 kJ/mol, respectively, are calculated. Hence, for the same large Si/Al ratio Brønsted sites in the faujasite lattice are predicted to be more acidic than in the ZSM-5 lattice. This difference is due to differences of both the local structures (including the structure relaxation) and the crystal potentials. No correlation is found between T−O−T bond angles or $^1$H NMR chemical shifts and heats of deprotonation.

## 1. Introduction

The protonated forms of zeolites are solid Brønsted acids. They are used as catalysts in petrochemical processes but also for the conversion of methanol to gasoline or to olefins.[1] The origin of the Brønsted acidity is a proton which compensates the negative charge of an $AlO_4^-$ tetrahedron in a zeolite framework. The proton can be attached to any of the four oxygen atoms of the $AlO_4^-$ tetrahedron, and the Al can be in any of the crystallographically different tetrahedral (T) sites of the zeolite framework. Brønsted sites are identified by IR spectroscopy (characteristic OH stretch band) and $^1$H NMR spectroscopy. The acidity of zeolite catalysts is characterized by measuring the strength of their interaction with base molecules such as ammonia. Techniques applied are temperature-programmed desorption and heat flow microcalorimetry.[2]

What one would like to understand is how different factors such as the aluminum content and the local structure affect the acidity. While in experiments it is not always easy to separate the different factors, quantum mechanical techniques are ideally suited to study the relation between the structure and reactivity of zeolitic Brønsted sites. These theoretical techniques are also ideally suited to analyze the relation between different measured parameters and the acid strength. For gas-phase molecules, by definition, acid strength is the enthalpy of deprotonation. Available acidity scales are based on measured proton-transfer equilibria and entropy estimates.[3] For solid acids such as zeolites the enthalpy of deprotonation cannot be directly measured. However, quantum mechanical calculations are possible and can provide fundamental data on the acid strength of zeolitic Brønsted sites which are not easily accessible by experiments.

Previous studies of zeolite acidity and spectroscopic properties used finite cluster models.[4,5] They provided valuable data on the average position of zeolitic Brønsted sites on a general acidity scale, they helped to assign vibrational spectra and NMR spectra, and they revealed the relationship between spectroscopic properties and acid strength.[6] Cluster models have two limitations: (i) They are treated like molecules in the gas phase and therefore allow for a relaxation of the atoms on deprotonation which is not as constrained as would be the case if the Brønsted site were part of the periodic solid. (ii) They neglect the long-range potential of the periodic solid. This means cluster models do not discriminate between Brønsted sites in different crystallographic positions or in different frameworks. If we would like to address these problems, we have to look for other methods. Periodic ab initio calculations of zeolite catalysts include all these effects from the beginning. Unfortunately, their use is limited because of the enormous computational effort arising from the large size of the unit cell and the low space group symmetry of most of the zeolite catalysts.[7−11] To our knowledge the only optimization of a protonated form of a zeolite has been reported by Nicholas and Hess[10] for a sodalite with 38 atoms in a unit cell and the space group $P\bar{1}$. Six degrees of freedom belonging to the atoms of the acid site have been optimized. Density functional calculations employing plane

† Dedicated to Sir John Meurig Thomas on the occasion of his 65th birthday.

* To whom correspondence should be addressed.

⊗ Abstract published in *Advance ACS Abstracts,* November 1, 1997.

S1089-5647(97)01779-3 CCC: $14.00 

wave basis sets find increasing use,[12−14] but their application to zeolite catalysts with unit cells as large as ZSM-5 is still an enormous computational task.

We developed an alternative technique that corrects for the defects of the cluster model.[15] We combine the quantum mechanical ab initio description of the cluster model (QM) with a description of the periodic zeolite structure by an interatomic potential function (Pot). In this combined computational scheme (QM−Pot) the atoms of the active site "feel" that they are part of the periodic solid. The long-range interactions are included at the level of the interatomic potential function. Since the interatomic potential is a shell model ion pair potential, polarization effects are included. The parameters of the shell model potential are derived from ab initio calculations. Our method differs from other schemes[16,17] by details of handling the hydrogen atoms introduced for terminating the cluster. Previously, attempts have been made to improve cluster calculations by fixing the boundary atoms of the cluster to positions they have in the periodic lattice[18−23] and by including the potential of the periodic lattice in some approximate way.[19−21,23]

While all these studies deal with a selected site in a given framework, either ZSM-5 or faujasite, for the first time we provide a comparison of Brønsted sites in different frameworks. We study high-silica H-faujasite and H-ZSM-5 which contain 145 and 289 atoms in the unit cell, respectively. We use the embedding scheme to make structure predictions for these catalysts protonated at different crystallographic sites and compare their stabilities and acidities. Once the structure is obtained, $^1$H NMR chemical shifts and OH stretching vibrational frequencies are calculated. The catalytic activity of the zeolite catalysts is characterized by their energy of deprotonation, $\Delta E_{DP}$, which is easily accessible by quantum chemical methods.[24]

$$Z{-}OH \rightarrow Z{-}O^- + H^+ \qquad (1)$$

Since it is defined as the energy difference between the deprotonated system (the anionic zeolite framework Z−O$^-$) and the protonated zeolite Z−OH, it requires an embedded cluster calculation with full structure relaxation not only for the parent system but also for the deprotonated system. This creates a number of technical problems, which are discussed in the Methods part: The potential functions used for the parent system and the deprotonated system are different, and a divergent Coulomb term appears in the energy of a lattice with a negative charge in every unit cell.

## 2. Methods

**2.1. The Embedding Scheme.** The present embedding scheme partitions the system studied (S) into two parts, the inner region (I) and the outer region (O). The inner region is identical with the part of interest of the zeolite, e.g. the Brønsted site. It is described quantum mechanically. If the inner region is chemically bonded to the outer region, partitioning implies the breaking of bonds and leads either to a charged or to a high-spin system which would only poorly represent the solid.[25] For this reason the dangling bonds of the inner part are saturated with hydrogen atoms, which are called link atoms. The inner part and the link atoms form the cluster (C), and the inner part and the outer part build the host, which is identical with the entire system (S). The periodic host structure (S) is described by an analytical potential function. Figure 1 shows the definition of inner region (I), link region (L), and outer region (O) for a cluster consisting of two $TO_4$ tetrahedra ([T,T] model).

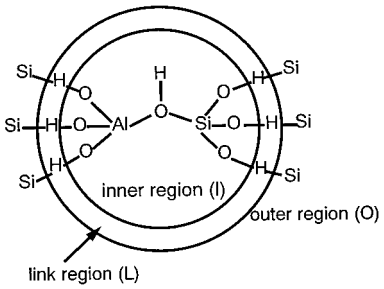


**Figure 1.** Definition of a di-tetrahedra cluster, [T,T], for the acidic Brønsted site.

The total energy, $E$(S), and the forces acting on the atoms, $F_\alpha$(S), are obtained as follows:[15]

$$E(S) = E_{QM}(C) + E_{Pot}(S) - E_{Pot}(C) \qquad (2a)$$

$$F_\alpha(S) = F_{\alpha,QM}(C) + F_{\alpha,Pot}(S) - F_{\alpha,Pot}(C) \qquad \alpha \in I \qquad (2b)$$

$$F_\beta(S) = F_{\beta,Pot}(S) \qquad \beta \in O \qquad (2c)$$

To the quantum mechanical results for the cluster, $E_{QM}$(C) and $F_{\alpha,QM}$(C), the results of the periodic description of the lattice by the interatomic potential, $E_{Pot}$(S) and $F_{\alpha,Pot}$(S), are added. The third contribution, $E_{Pot}$(C) and $F_{\alpha,Pot}$(C), results from the application of the interatomic potential function to the cluster. Its subtraction eliminates approximately (i) the double counting of contributions coming from atoms in the inner region since they are included both in $E_{QM}$(C) and in $E_{Pot}$(S) and (ii) contributions from the link atoms which are not present in the real solid.

For an atom $\alpha$ of the inner region, all three terms contribute to the force on the atom. For an atom $\beta$ of the outer region, the force is obtained from the interatomic potential function alone. A link atom is not moved according to the force acting on it. It is instead kept fixed on the bond which it terminates. Since the link atom positions depend on the positions of the real atoms of the corresponding bond, they create small contributions to the forces on the real atoms (see ref 15 for details).

It should be noted that the three energies of eq 2a are not directly comparable, since the energies evaluated using the interatomic potential functions are determined only up to an additive constant which depends on the parametrization and the size of system. Hence, energies calculated with this embedding scheme are only comparable if clusters of the same size are embedded in periodic structures of the same unit cell composition and if the same interatomic potential function is used. Of course, this is the case for zeolites that are protonated at different crystallographic sites. Relative energies such as deprotonation energies and calculated properties can be also compared for different zeolite frameworks.

The implementation[26] used in this study describes the outer part and the interactions between the outer and the inner part by an ab initio parametrized ion pair shell model potential.[27] All parameters of this potential were fitted to energies, gradients, and force constants of cluster models,[27] which were calculated using the same method (Hartree−Fock) and the same basis set as used in the embedding calculations. Potential functions derived from experimental data are not suitable because they do not provide parameters for the link atoms which do not exist in the real system and also because there is a lack of experimental data for the local structure of the Brønsted sites. The ab initio calculations for the cluster are made in the HF approximation using the program TURBOMOLE.[28]

**2.2. Application to Deprotonation Reactions.** The ab initio shell model potential derived for zeolites[27] assigns different atom types to the active site atoms in the protonated and deprotonated state, i.e. Si−$O_b$($H_b$)−Al on the left-hand side and Si−O−Al on the right side of reaction 1. In the case of classical potential calculations the reaction energy is determined only up to a constant since both the left-hand side and the right-hand side energies include additive constants which can be different. However, we will show that within our embedding scheme this has only little effect on the contribution of the potential to the total QM−Pot deprotonation energy.

The deprotonation energy is defined as

$$\Delta E_{DP} = E(Z{-}O^-) - E(Z{-}OH) \tag{3}$$

If we apply the embedding scheme (eq 2a) to both Z−OH and Z−$O^-$, and introduce the notation CH, SH and $C^-$, $S^-$ for the cluster and the total system of the protonated and the deprotonated form, respectively, we obtain

$$\Delta E_{DP} = E_{QM}(C^-) + E_{Pot}(S^-) - E_{Pot}(C^-) - [E_{QM}(CH) + E_{Pot}(SH) - E_{Pot}(CH)]$$

$$= \Delta E_{QM} + \Delta E_{Pot} \tag{4a}$$

$$\Delta E_{QM} = E_{QM}(C^-) - E_{QM}(CH) \tag{4b}$$

$$\Delta E_{Pot} = E_{Pot}(S^-) - E_{Pot}(C^-) - [E_{Pot}(SH) - E_{Pot}(CH)] \tag{4c}$$

We decompose the shell model potential energies into contributions coming from the outer region (O), the link atoms (L), the inner region (I), and their interactions. Three-body terms are neglected. The protonated and the deprotonated systems differ by their inner regions only, which we denote IH and $I^-$, respectively. Since the energies of the protonated and deprotonated forms are calculated at their respective equilibrium structures, we introduce a notation such as IH//SH, which means a contribution from the inner region only, calculated "at the structure of" the whole system (periodic zeolite) and using the potential function with parameters for the whole protonated system. Further, terms such as O−IH//SH denote an interaction between two regions. Then, for the left-hand side of the reaction,

$$SH = O//SH + IH//SH + O{-}IH//SH \tag{5a}$$

$$CH = L//SH + IH//SH + L{-}IH//SH \tag{5b}$$

and for the right-hand side

$$S^- = O//S^- + I^-//S^- + O{-}I^-//S^- \tag{5c}$$

$$C^- = L//S^- + I^-//S^- + L{-}I^-//S^- \tag{5d}$$

Taking the difference between the host and cluster energies according to eq 2a, the potential contributions belonging to the inner region and the proton alone vanish.

$$SH - CH = O//SH - L//SH + O{-}IH//SH - L{-}IH//SH \tag{6a}$$

$$S^- - C^- = O//S^- - L//S^- + O{-}I^-//S^- - L{-}I^-//S^- \tag{6b}$$

On the assumption that the structures of the outer and the link regions of the system with and without the proton are the same (O//SH = O//$S^-$ and L//SH = L//$S^-$) we obtain the contribution of the potential to the deprotonation energy by applying eq 6 to eq 4c:

$$\Delta E_{Pot//QM-Pot} \approx E(O{-}I^-//S^-) - E(O{-}IH//SH) - [E(L{-}I^-//S^-) - E(L{-}IH//SH)] \tag{7}$$

If the cluster is large enough that the structural distortion upon deprotonation decays within the cluster region, the short-range terms at the boundaries between I and L and I and O are the same for SH and $S^-$. Equation 7 then consists only of electrostatic interactions, i.e. long-range contributions:

$$\Delta E_{Pot//QM-Pot} \approx \Delta E_{LR//QM-Pot} \tag{8}$$

Hence,

$$\Delta E_{DP} \approx \Delta E_{QM//QM-Pot} + \Delta E_{LR//QM-Pot} \tag{9}$$

This equation reflects that embedding has two effects: (i) the quantum mechanical cluster calculations are performed at the respective structures obtained by embedding, $\Delta E_{QM//QM-Pot}$. (ii) The potential function used provides a long-range correction to the deprotonation energy calculated, $\Delta E_{LR//QM-Pot}$.

Moreover, accepting that the potential provides a long-range correction which depends on the charges of the atoms and the shells and their positions only means that the use of different shell model potentials for the protonated and deprotonated structures does not create a problem. Since the same formal charges are assigned to $O_b$ and O, the potential change does not influence $\Delta E_{LR//QM-Pot}$.

**2.3. Deprotonation and Periodicity.** Applying periodic boundary conditions to the deprotonation process—as we do in our embedding scheme (eqs 2)—means that a negative charge is created in every unit cell. Not only does this create a formal problem insofar as a divergent Coulomb term appears in the energy of the deprotonated lattice but it is also an unrealistic model. In a catalytic process we do not expect release of a proton in every unit cell at the same time.

Suggestions have been made for approximate solutions of both problems. The divergence of the Coulomb energy is eliminated by adding a uniform positive background charge to the deprotonated unit cell.[29,30] The interaction between the charged defects in different unit cells in the presence of a uniform background charge is eliminated using a macroscopic approximation.[29] We may expect that these approximations, which are based on multipole expansions for charge distributions, work best for large unit cells as the zeolite catalysts have. The applicability of the approximations can be easily checked by doubling the unit cell size. The Coulomb energy of a periodically repeating array of charges immersed in a neutralizing background (jellium), $E_{Coul,periodic}$, is obtained by adding a correction term, $E_{BC}$[29,30] (BC: background charge), to the Ewald energy, $E_{Ewald}$, of the interacting core and shell species in the periodic shell model potential calculation:

$$E_{Coul,periodic} = E_{Ewald} + E_{BC}$$

$$E_{BC} = -\frac{1}{2}\frac{\pi Q^2}{V\eta} \tag{10}$$

$Q$ is the net charge of the unit cell given as the sum of the charges of all ions and shells, $V$ is the volume of the unit cell, and $\eta$ is the Ewald screening parameter. For unit cells as large as zeolites the compensation term is usually small ($E_{BC}/E_{Coul,periodic} < 0.0001$), but its inclusion is essential. Since the correction term $E_{BC}$ does not depend on the positions of the

ions and shells, it has no effect on the forces, but it is not invariant to changes of the unit cell volume induced by strains of the lattice. To obtain the constant pressure structure of the anionic zeolite framework, the first and second strain derivatives of $E_{BC}$ must be included. They are given in the Appendix. Equations 10 and A1−A3 were implemented into the GULP program.[31]

From the QM−Pot energies of the neutralized deprotonated framework and the protonated zeolite an estimate of the energy for the periodic deprotonation of a zeolite is obtained, i.e. for the case when the proton is removed in every single unit cell. This is a rather unrealistic situation, and one is interested in the deprotonation of a single site in an otherwise perfect infinite crystal. The difference between the energy per unit cell for the two situations—periodic defect and isolated defect—is the interaction between the charges generated by proton removal. It is equivalent to the electrostatic interaction between the protons. As proposed by Leslie and Gillan,[29] this can be treated by a macroscopic approximation if the repeating unit of the periodic defects is large. The compensation is obtained as the Coulomb energy of a periodic array of protons with a neutralizing background immersed in a structureless dielectric, whose dielectric constant, $\epsilon_0$, is equal to that of the perfect protonated zeolite. The potential function deprotonation energy of a zeolite which releases a single proton is then

$$\Delta E_{DP}^{Pot,single} = \Delta E_{DP}^{Pot,periodic} - \frac{E_{Coul,periodic}(H^+)}{\epsilon_0} \qquad (11)$$

$E_{Coul,periodic}(H^+)$ is obtained by a shell model potential calculation applying the usual Ewald summation techniques on an array of protons ordered as in the perfect protonated zeolite. The dielectricity constant, $\epsilon_0$, is calculated as one-third of the trace of the static dielectric tensor obtained from a shell model potential calculation of the protonated zeolite.

## 3. Details of Calculations

**3.1. Quantum Mechanical Calculations for the Active Site Cluster.** For silicon, aluminum, and hydrogen double-zeta plus polarization (DZP) basis sets were used. For the oxygen atoms, a triple-zeta valence plus polarization (TZP) basis set was employed.[32] For the Si, Al/O/H atoms the (11s,7p)/(9s,5p)/(4s) Gaussian primitive sets were taken from Huzinaga[33,34] and contracted into the following pattern {521111,4111}/{51111,-311}/{31}. Polarization functions with the exponents 0.4 (Si), 0.3 (Al), 1.2 (O), and 0.8 (H) were added. This basis set, named T(O)DZP, was used in many previous studies of this laboratory. When defining the cluster models, the cutout was made such that the clusters terminate with OH groups. For OH groups bonded to silicon/aluminum the fixed link atom distance $r_{OH}$ was set to 0.945/0.940 Å. These values were obtained by free cluster optimizations with the same basis set.[35] All SCF calculations were carried out in $C_1$ symmetry.

**3.2. Shell Model Potential Calculations for the Framework.** The program GULP[31] is used for evaluating the shell model contribution of the periodic structure. The summation of the long-range Coulomb interactions is made by the Ewald technique. Short-range interactions between the ions are considered up to a cutoff distance of 10 Å.

The structure optimizations by the embedded cluster technique were made with fixed unit cell parameters. These parameters were determined by a lattice energy minimization using the same potential function as used in the embedded cluster calculation. This procedure has the advantage that the starting positions of the atoms of the periodic structure, especially those which do not belong to the cluster, are already close to the final atom positions obtained by the embedded cluster calculation. This reduces the number of iterations of the structure optimization process.

**3.3. Calculations of Vibrational Frequencies.** The O−H stretching vibrational frequencies were calculated in the harmonic approximation. The harmonic force constant was obtained from the energies of five equally spaced points on the potential curve along the distorted O−H bond (step size 1 pm). The neglect of the coupling of the OH mode with the other modes leads to an error of about 3 $cm^{-1}$, which is certainly negligible considering the error of the harmonic approximation and HF method. The usual scale factor of 0.89 was applied to the calculated results to correct the error of the HF and the harmonic approximation.

Below we will occasionally use frequencies obtained with the QM method at the equilibrium structure found by the QM−Pot technique. This means calculating force constants outside the minimum of the quantum mechanical PES. It is known[36] that such an approach can lead to improved results since an improved structure is used and harmonic frequencies are, in first approximation, determined by the structure.

**3.4. Calculation of Proton NMR Chemical Shifts.** The $^1$H NMR chemical shifts were calculated for cluster models at the structures obtained by the combined QM−Pot scheme for the embedded cluster approach. Hence the influence of the crystal environment on the chemical shift is indirect, via the structure. Since chemical shifts are structure sensitive, this procedure is expected to include the major effects. Hence the clusters used for the shift calculation in general are different (larger) from that used for getting the structures. However, long-range electrostatic effects are also known to affect the shielding (see, for example, ref 37). Therefore, clusters of increasing size were cut out from the optimized structures until convergence of the calculated chemical shifts was achieved. The chemical shifts were calculated within the HF approximation using gauge-including atomic orbitals (GIAO) as implemented in the SHEILA module of the TURBOMOLE program.[38] A TZP basis set was used.[39] Following ref 40 the methanol molecule was adopted as internal secondary standard for conversion from the calculated isotropic absolute shielding constants $\sigma$ to the chemical shift with respect to TMS, $\delta_{TMS}$.

$$\delta_{TMS}(\text{Cluster}) = \delta_{TMS}(CH_3OH) + \sigma(CH_3OH) - \sigma(\text{Cluster}) \qquad (12)$$

The calculated absolute SCF shielding constant, $\sigma(CH_3OH)$, was 32.7 ppm for the SCF-optimized structure,[40] while the experimental gas-phase value, $\delta_{TMS}(CH_3OH)$, is 0.02 ppm.[41]

## 4. H-Faujasite

**4.1. Models Considered.** The faujasite structure is made of sodalite cages connected by double six-rings (Figure 2). The primitive cell used in our calculations consists of two such sodalite cages. Silica−faujasite has only one tetrahedral site in its asymmetric unit. The H-form studied contains one acidic site per unit cell. This corresponds to a silicon/aluminum ratio of 47. This very low aluminum content permits the investigation of the properties of an isolated acidic site.

For all four sites di-tetrahedra clusters, [T,T], were embedded in the periodic lattice (see Figure 3); that is, clusters and hosts are of the same size for all four sites. To investigate the influence of the cluster size, five different four-ring models, [R-4T], were used. Only two different types of four-rings exist in the faujasite structure (Figure 4). One includes the oxygen

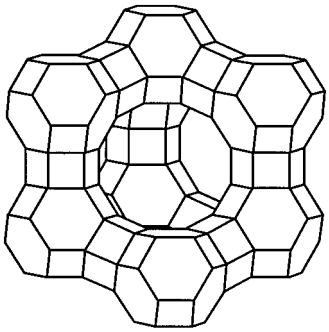

**Figure 2.** Faujasite framework. For simplicity only the positions of the tetrahedral atoms are shown.

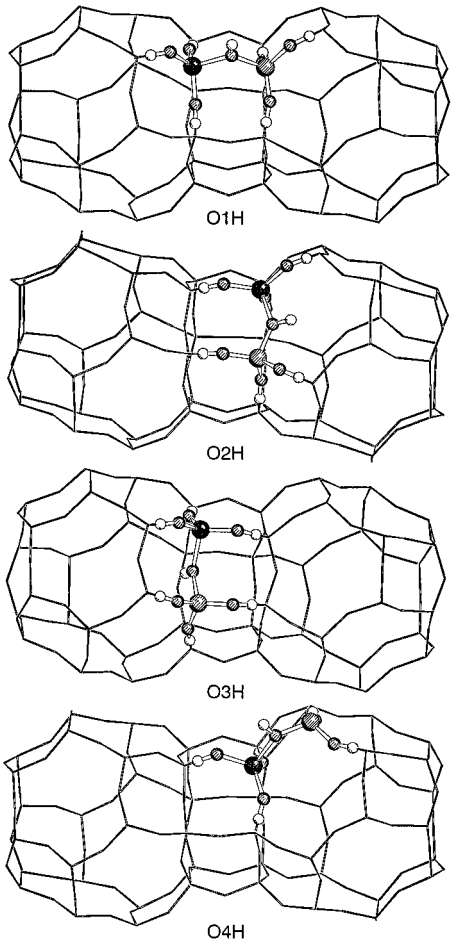


**Figure 3.** Di-tetrahedra models for the different acidic sites of faujasite. From top to bottom: proton attached to framework oxygen at the O1, O2, O3, and O4 positions, respectively.

positions O1, O3, O1, and O2. This model is referred to as model A. The other contains the O3, O4, O2, and O4 positions and is named model B. Hence, only model A can be used to study the O(1)H site and only model B to study the O(4)H site, but both four-ring models can be used to study the O(2)H and O(3)H sites. For the O(3)H site both were indeed adopted. Comparison of the results provides an estimate of the errors made with the embedding scheme. For the O(3)H site a six-ring model was also employed to investigate the possible occurrence of a hydrogen bond in this six-ring (vide infra, Figure 6).

**4.2. Relative Stabilities of Different Sites.** Table 1 shows the relative energies of the four different Brønsted sites of faujasite. Besides the results of the embedded cluster calculations the relative energies obtained by two different shell model potentials alone are given. The ab initio shell model potential

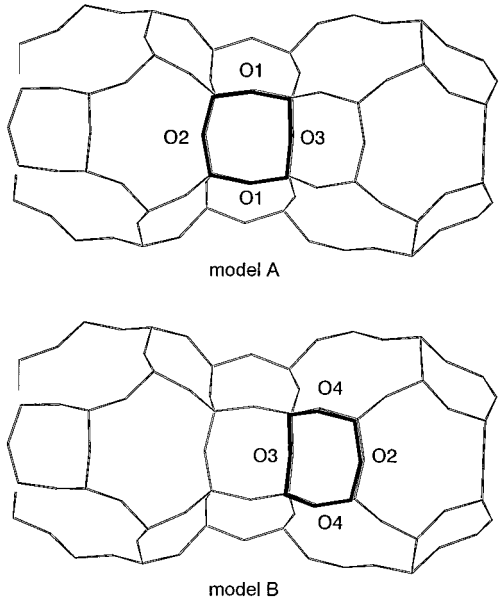


**Figure 4.** The two possible four-ring models for faujasite.

**TABLE 1: Relative Energies (kJ/mol) of the Four Bridging Hydroxyls in H-Faujasite (Si/Al = 47)**

| | O(1)H | O(2)H | O(3)H | O(4)H |
|---|---|---|---|---|
| empirical shell model[a] | 0.0 | 14.5 | −5.3 | 18.4 |
| ab initio shell model[b] | 0.0 | 9.2 | −8.8 | 19.1 |
| embedded cluster [T,T] | 0.0 | 28.7 | 4.6 | 22.6 |
| embedded cluster [R-4T] | 0.0 | 23.9 | 4.4 | 22.9 |

[a] Reference 44. [b] Reference 27.

is the same as that used in the present embedded cluster (QM−Pot) calculations. All calculations predict that the proton positions at O1 and O3 are the most stable ones. The energetic sequence within the O1−O3 and O2−O4 subsets changes when passing from the pure shell model potential calculations to the combined QM−Pot calculations. The error of the QM−Pot calculations can be estimated by comparing the results for the embedded clusters of different sites, [T,T] and [R-4T]. The largest deviation is 4.8 kJ/mol for the O(2)H site; all other deviations are below 0.5 kJ/mol. Another accuracy check is possible by comparing the energy difference calculated for the two four-ring models. The difference between the two energies for the O(3)H site obtained for the [R-4T] models A and B is a mere 0.7 kJ/mol. We conclude that the error of relative energies made by applying the present QM−Pot scheme is not larger than about 5 kJ/mol.

Although the energy difference between the O(1)H and O(3)H sites is within this range, the prediction that the O(1)H site is the more stable one is assumed to be significant because the predictions of the embedded di-tetrahedra and four-ring clusters for this difference agree within 0.2 kJ/mol. This prediction is also in agreement with a previous neutron diffraction study (for higher Al concentration)[42] which reached the conclusion that the proton occupation is 8:2:4 at the O1:O2:O3 positions. It was also observed that the low-frequency (LF) band in the IR spectra which is assigned to the O(3)H site vanishes at lower proton concentration.[43] These experimental results cannot be directly compared with the calculated ones since they were obtained for different Si/Al ratios and $Na^+$ ions were present for charge compensation in addition to protons. However, because of the small energy difference, a definitive answer must await more accurate periodic calculations which include correlation effects.

**4.3. Deprotonation Energies.** For the determination of the deprotonation energies, deprotonated di-tetrahedra models were

**TABLE 2: Absolute Deprotonation Energies, $\Delta E_{DP}$, Dielectric Constants, $\epsilon_0$, and Interaction Energy of the Charged Defects, $E_{Coul,periodic}(H^+)/\epsilon_0$, for Different Brønsted Sites in H-Faujasite: Embedded [T,T] Cluster Calculations (Relative Energies with Respect to O(1)H Are Given in Parentheses; Energies in kJ/mol)**

| | O(1)H | O(2)H | O(3)H | O(4)H |
|---|---|---|---|---|
| $\epsilon_0$ | 2.382 | 2.372 | 2.362 | 2.384 |
| $E_{Coul,periodic}(H^+)/\epsilon_0$ | −54.2 | −54.4 | −54.7 | −54.3 |
| $\Delta E^{QM//QM-Pot}$ | 1369.1 | 1353.1 | 1344.2 | 1380.4 |
| $\Delta E^{LR//QM-Pot}$ | −118.8 | −126.8 | −96.7 | −153.6 |
| $\Delta E_{DP}$ | 1250.3 | 1226.3 | 1247.4 | 1226.8 |
| | (0.0) | (24.0) | (2.9) | (23.5) |

embedded at the four oxygen positions of the anionic faujasite framework. Table 2 shows the results obtained with the QM−Pot scheme. The relative deprotonation energies with respect to the O(1)H site are given in parentheses. Since deprotonation of the four different O($n$)H sites yields one and the same deprotonated faujasite structure, the relative deprotonation energies are at the same time relative stabilities of the four O($n$)H sites. The higher the deprotonation energy, the more stable the O($n$)H site. The numbers reported in Table 2 are slightly different from that in Table 1 for the embedded di-tetrahedra clusters (largest difference 4.7 kJ/mol for O(2)H). The reason is that we used four different di-tetrahedra models for the anionic framework with O(1) to O(4) as bridging atoms. If our QM−Pot scheme were perfect, all four calculations should give the same energy and the results for the [T,T] clusters in Table 1 and for the relative deprotonation energies in Table 2 would be identical. This means that the differences between the two sets of results are another indication of the accuracy of the embedding scheme. In agreement with our above conclusion, these errors are smaller than 5 kJ/mol.

The absolute deprotonation energies contain a term introduced to eliminate interactions between protons in different unit cells (eq 11). It is also shown in Table 2 together with the calculated dielectric constants. Its contribution to the QM−Pot deprotonation energies is 54−55 kJ/mol (∼4.6%), which is considerable. To assess the validity of the macroscopic approximation used, we performed a shell model potential lattice energy minimization of a 2 × 1 × 1 supercell of faujasite which contained 96 T atoms and had the same Si/Al ratio as the primitive cell. One active site was protonated, whereas the other was not, and therefore the distance between two deprotonated sites was doubled in one lattice direction. Due to the cell doubling the compensation term decreases by 16.8 kJ/mol and $\Delta E_{DP}^{Pot,periodic}$ increases by 18.3 kJ/mol. The net effect is only 1.6 kJ/mol, so that the deprotonation energies for the removal of one single proton are nearly equal for the single and double cells. The remaining small energy difference is probably due to the different structural relaxation when one or two acid sites are deprotonated in the 2 × 1 × 1 supercell.

The long-range contribution of the shell model potential to the deprotonation energy for the embedded di-tetrahedra clusters is substantial, about 9.5% or −119 kJ/mol (site O(1)H). With increasing cluster size this term should decrease and the quantum mechanical contribution should increase. The stability of the final QM−Pot results toward an extension of the cluster is an important requirement for a reliable embedding scheme. Therefore clusters of increasing size were used for a given structure. First, a tri-tetrahedra cluster, [T,T,T], was embedded including sites O(1)H and O(4) at bridging positions, and complete structure optimizations were made for the protonated and deprotonated systems using the embedding scheme. Compared to the embedded [T,T] cluster the total QM−Pot deprotonation energy changed by less than 2 kJ/mol, although the contribution

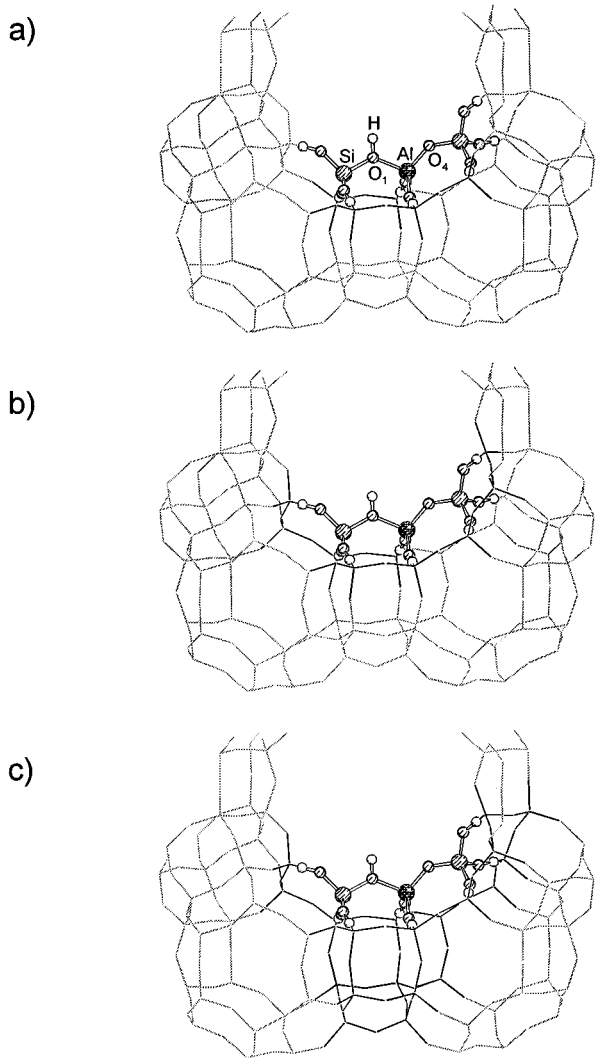


**Figure 5.** Tri-tetrahedra model embedded in faujasite such that oxygen sites O1 and O4 are in the bridging positions. Proton at O1. Dark lines: Clusters of increasing size embedded at the same lattice position. (a) FAU-$4^3$ (shell-3), (b) FAU-$4^5$, (c) shell-5 (see text for nomenclature).

of the potential changed by 17 kJ/mol. These structures were adopted for single-point calculations on embedded clusters of increasing size (Figure 5). The next larger model includes three coordination shells around the central aluminum atom (shell-3.0). If two terminating hydroxyl groups were pointing to the same silicon atom of the outer region, this silicon atom was also included in the cluster and terminated with hydroxyl groups. Therefore our shell-3 model includes three connected four-rings, FAU-$4^3$. Adding another two shells of silicon and oxygen atoms yields the shell-5 model (1727 basis functions). An intermediate model between shell-3 and shell-5 is the FAU-$4^5$ model, which includes four coordination shells around the O1−Al−O4 group. The $4^5$ notation points to the fact that five four-rings are present. Figure 5 shows the protonated models and Table 3 the results. Although the long-range contributions of the potential converges slowly, the total QM−Pot energies are remarkably stable with increasing cluster size.

It is interesting to compare the embedded cluster results with results for cluster models that were optimized in free space. Using the same basis set, for the tri-tetrahedra model, [T,T,T], a deprotonation energy of 1296 kJ/mol is calculated. The data of Table 3 show that the structure constraints increase the quantum mechanical deprotonation energy to 1354 kJ/mol when this model is embedded in the faujasite framework, and only long-range corrections make it as low as 1252 kJ/mol. It seems

**TABLE 3: Deprotonation Energies, $\Delta E_{DP}$ (kJ/mol), for the O(1)H Site of H-Faujasite: Convergence of the Embedded Cluster Result with Increasing Cluster Size**

| | $\Delta E_{DP}$ | | |
|---|---|---|---|
| embedded model | $\Delta E_{QM/QM-Pot}$ | $\Delta E_{LR//QM-Pot}$[a] | $\Delta E_{QM-Pot}$ |
| [T,T] | 1369.1 | −118.8 | 1250.3 |
| [SiO$^1$AlOSi] = [T,T,T] | 1353.7 | −101.8 | 1251.9 |
| FAU-4$^3$//[T,T,T] | 1331.3 | −78.2 | 1253.1 |
| FAU-4$^5$//[T,T,T] | 1334.5 | −81.5 | 1253.1 |
| shell-5//[T,T,T] | 1302.8 | −51.7 | 1251.1 |

[a] Long-range contribution of the potential, $\Delta E_{LR} = \Delta E(S) - \Delta E(C)$.

that in free space clusters structural relaxation is partially compensating for missing long-range effects. This explains why free space cluster models have been successful in the past in spite of the complete neglect of long-range effects.

**4.4. Structures.** The lattice constants obtained by energy minimization with the ab initio parametrized shell model potential do not change much upon deprotonation, which indicates that the structural distortions upon removal of a proton are localized around the active site. The lattice constants of the protonated and the deprotonated faujasites are included in the Supporting Information (Table S1). The optimized bond distances and angles for the different clusters embedded at the different crystallographic positions are listed in Table 4. Table 5 shows the corresponding results for the anionic faujasite framework. For comparison, with structures obtained by the shell model potential calculation only, which allows one to assess the quality of the ab initio shell model potential for deprotonated systems, we refer to Table 7 of ref 19. When fitting the parameters of the potential,[27] data of siliceous and protonated zeolite models were used, but not of deprotonated anionic models. The zeolite shell model potential seems to reproduce the Si−O bond lengths and the Si−O−Al bond angles well compared with the QM−Pot structures for the embedded di-tetrahedra clusters, whereas it overestimates the Al−O distances by 0.012−0.019 Å. Upon deprotonation, large structure changes occur for the Si−O and Al−O bond lengths and the Si−O−Al angles, as comparison of the data in Tables 4 and 5 reveals. The largest changes are observed for the Al−O−Si angles, which increase by 8−14°. These large variations are easily accommodated by the zeolite framework due to the flexibility of the T−O−T angles.

**4.5. OH Frequencies.** Tables 6 and 7 show the O−H frequencies of the embedded di-tetrahedra and four-ring models, respectively. The vibrational frequencies were calculated for all four PESs which occur in the embedding scheme (eq 2). The quantum mechanical cluster calculation carried out at the structure obtained by the QM−Pot calculations (QM//QM−Pot) leads to four different frequencies for the four O(*n*)H groups. Since the value of the O−H frequency is mainly determined by the O−H bond length, the effect of the periodic structure is included in the quantum mechanical cluster calculations via its effect on the OH equilibrium distance. These frequencies show the sequence O(1)H > O(4)H > O(3)H > O(2)H. The direct long-range correction by the shell model potential, Pot(S)//QM−Pot − Pot(C)//QM−Pot, reduces the frequencies. The quantum mechanical cluster frequencies calculated at the QM−Pot equilibrium structures show the least changes when passing from the [T,T] to the [R-4T] models. Therefore they are considered the most reliable predictions.

The experimental vibrational spectrum of H-faujasite (Si/Al = 23) shows two characteristic OH bands, the so-called HF (high-frequency) band at 3623 cm$^{-1}$ and LF (low-frequency) band at 3550 cm$^{-1}$,[43] which are assigned to the O(1)H and the O(3)H acidic sites, respectively. After applying the common scale factor of 0.89 the frequencies calculated for the R-4T models, 3596 and 3537 cm$^{-1}$, reproduce very well the frequency difference between these two bands (cf. Table 13). For the LF band the average of the predictions for the two four-ring models A and B is taken.

**TABLE 4: Local Structure (Å, deg) of the Different Acidic Sites of H-Faujasite**

| position | model | *r*(Al−O) | *r*(Si−O) | *r*(O−H) | *r*(Al−H) | ∠(Al−O−Si) | ⟨*r*(Al−O)⟩[a] |
|---|---|---|---|---|---|---|---|
| | emb. [T,T] | 1.900 | 1.704 | 0.9558 | 2.478 | 125.8 | 1.756 |
| O(1)H | emb. R-4T | 1.905 | 1.701 | 0.9556 | 2.484 | 125.7 | 1.756 |
| | Fixed [T,T][b] | 1.989 | 1.689 | 0.9515 | 2.536 | 128.1 | 1.767 |
| | emb. [T,T] | 1.896 | 1.696 | 0.9618 | 2.379 | 137.7 | 1.759 |
| O(2)H | emb. R-4T | 1.903 | 1.695 | 0.9613 | 2.376 | 138.8 | 1.758 |
| | Fixed [T,T][b] | 1.970 | 1.680 | 0.9537 | 2.349 | 143.6 | 1.763 |
| | emb. [T,T] | 1.946 | 1.712 | 0.9619 | 2.468 | 132.2 | 1.764 |
| | emb. R-4T A | 1.952 | 1.709 | 0.9602 | 2.462 | 133.5 | 1.763 |
| O(3)H | emb. R-4T B | 1.952 | 1.709 | 0.9610 | 2.462 | 133.4 | 1.764 |
| | emb. R-6T | 1.943 | 1.706 | 0.9569 | 2.440 | 134.5 | 1.762 |
| | Fixed [T,T][b] | 1.968 | 1.677 | 0.9521 | 2.384 | 138.1 | 1.767 |
| | emb. [T,T] | 1.881 | 1.694 | 0.9576 | 2.424 | 131.1 | 1.757 |
| O(4)H | emb. R-4T | 1.885 | 1.691 | 0.9571 | 2.428 | 131.0 | 1.756 |
| | fixed [T,T][b] | 1.996 | 1.688 | 0.9527 | 2.492 | 134.4 | 1.767 |

[a] Average of all four Al−O bonds of the $AlO_4$ tetrahedron. [b] Positions of the terminating OH atoms fixed at positions given by the shell model optimization.

**TABLE 5: Deprotonated Di-tetrahedra Cluster Embedded at Different Oxygen Positions of Faujasite: Bond Lengths (Å) and Angles (deg) as Well as the Relative Total Energies of the Deprotonated Structures (kJ/mol)**

| position | model | *r*(Al−O) | *r*(Si−O) | ∠(Al−O−Si) | ⟨*r*(Al−O)⟩[a] | $\Delta E^{QM-Pot}$ |
|---|---|---|---|---|---|---|
| O1 | [T,T] | 1.733 | 1.571 | 136.7 | 1.742 | 0.9 |
| | potential only | 1.752 | 1.575 | 139.0 | | |
| O2 | [T,T] | 1.723 | 1.561 | 151.5 | 1.743 | 4.7 |
| | potential only | 1.737 | 1.565 | 151.5 | | |
| O3 | [T,T] | 1.751 | 1.575 | 147.3 | 1.744 | 1.8 |
| | potential only | 1.763 | 1.573 | 149.4 | | |
| O4 | [T,T] | 1.722 | 1.564 | 139.1 | 1.744 | 0.0 |
| | potential only | 1.739 | 1.570 | 141.5 | | |

[a] Average of all four Al−O bonds of the $AlO_4$ tetrahedron. Result of the periodic shell model calculation: 1.748 Å.

**TABLE 6: Uncoupled and Unscaled OH Stretching Frequencies of the Embedded [T,T] Models for the Different Acidic Sites of H-Faujasite ($cm^{-1}$)**

| potential surface[a] | O(1)H | O(2)H | O(3)H | O(4)H |
|---|---|---|---|---|
| QM(C)//QM−Pot(S) | 4039 | 3956 | 3956 | 4013 |
| Pot(C)//QM−Pot(S) | 4193 | 4188 | 4190 | 4183 |
| Pot(S)//QM−Pot(S) | 4159 | 4133 | 4111 | 4160 |
| QM−Pot(S) | 4003 | 3897 | 3872 | 3989 |

[a] Total potential energy surface, QM−Pot(S), and individual contributions defined by eq 2a.

**TABLE 7: Uncoupled and Unscaled OH Stretching Frequencies of the Embedded R-4T and R-6T Models for the Different Acidic Sites of H-Faujasite ($cm^{-1}$)**

| | | | O(3)H | | | |
|---|---|---|---|---|---|---|
| potential surface[a] | O(1)H | O(2)H | A | B | R-6T | O(4)H |
| QM(C)//QM−Pot(S) | 4041 | 3961 | 3980 | 3969 | 4010 | 4019 |
| Pot(C)//QM−Pot(S) | 4184 | 4193 | 4188 | 4190 | 4216 | 4181 |
| Pot(S)//QM−Pot(S) | 4160 | 4149 | 4138 | 4135 | 4187 | 4164 |
| QM−Pot(S) | 4016 | 3914 | 3928 | 3910 | 3980 | 4002 |

[a] Total potential energy surface, QM−Pot(S), and individual contributions defined by eq 2a.

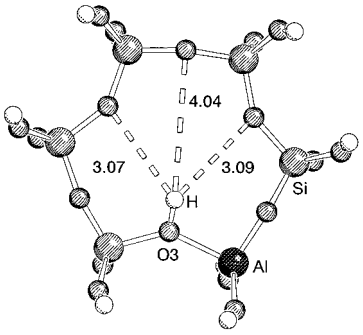


**Figure 6.** Optimized structure of the embedded six-ring model for the O3H site of faujasite.

Since the O(3)H proton site points directly into a six-membered ring, the lower OH frequency of this site compared to that of the O(1)H site was explained by a weak hydrogen bond of the acidic proton with an oxygen atom placed on the opposite site of the six-membered ring, e.g., ref 45 and references quoted therein. To check the possible existence of such a weak hydrogen bond, a six-membered ring (Figure 6) was defined as an embedded cluster which includes the possible hydrogen bond in the QM part. No significant change of the structure is found compared with the smaller models. The oxygen atom in the direction of the OH group on the opposite ring side is farther apart from the proton than all the other oxygen atoms in the six-membered ring. The distances to the two oxygen atoms which are next nearest neighbors of the protonated oxygen atom are also larger than typical hydrogen bond distances. Although there is no indication of a hydrogen bond, the large change of the calculated frequency of 54 $cm^{-1}$ between the [T,T] cluster model and the six-membered ring model shows that the chemical environment in the six-membered ring is different from that of the supercage.

There is another explanation for the frequency difference between the HF (O(1)H) and LF band (O(3)H): A correlation exists between the OH frequency and the Si−O(H)−Al bond angle.[44] To check this hypothesis, calculations were made on a small di-tetrahedra model saturated with hydrogen atoms (Figure 7). The saturation with hydrogen atoms prevents the formation of internal hydrogen bonds in the free space optimization, which is a problem with OH-saturated models. The structure of the $H_3SiO(H)AlH_3$ model was optimized for fixed

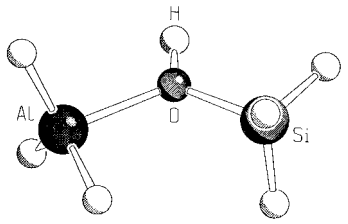


**Figure 7.** $H_3SiOH{\cdot}AlH_3$ model used for free space structure optimization.

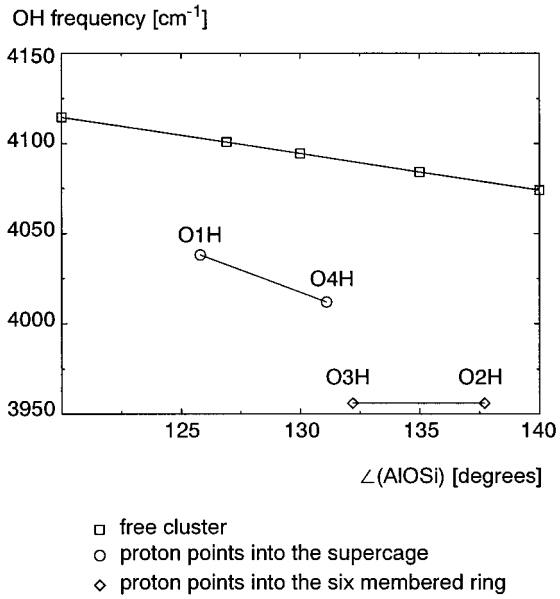


**Figure 8.** Dependence of the OH stretching frequencies on the AlOSi bond angle. Embedded cluster results for the four acidic sites in faujasite and free space optimization of the $H_3SiOH{\cdot}AlH_3$ cluster for different Si−O−Al angles.

values of the Al−O−Si angle between 120° and 140°. For these relaxed structures the vibrational harmonic frequencies were determined using the FORCE module of the TURBOMOLE program. A linear dependence of the OH frequency on the Si−O−Al angle is found (Figure 8, correlation coefficient −1.0). Figure 8 shows also the O−H stretching frequencies calculated for the embedded [T,T] clusters (QM(C)//QM−Pot result). The frequencies of the four sites form two subsets with a similar dependency. One set consists of the O(1)H and O(4)H sites, the protons of which point into the supercage. The protons of the O(2)H and O(3)H sites which belong to the other set point into a six-membered ring. The different chemical environment is thus also reflected by the vibrational frequencies. Although the frequencies are calculated with the finite cluster model, the structure of the cluster is determined by the combined QM−Pot scheme and, hence, influenced by long-range interactions. We conclude that the differences between the LF and HF band cannot be explained by local effects such as H-bond formation or bond angle correlation.

**4.6. $^1$H NMR Chemical Shifts.** The chemical shift of the protons at the different hydroxyl sites was calculated for the structures obtained by the embedded cluster calculations. Figure 9 shows the cluster models cut out from the optimized structures for this purpose. The series of models starts with the di-tetrahedra and four-ring models since these were used for the structure optimization. The FAU-$4^3$ model consists of three four-rings (cf. Figure 5), while in the FAU-$6^1 4^3$ cluster one six-ring is connected with three four-rings. Table 8 lists the calculated shifts. The label [T,T]//[R-4T] denotes a di-tetrahedra cluster, [T,T], used for the chemical shift calculation which is cut out from a structure obtained by embedding a four-

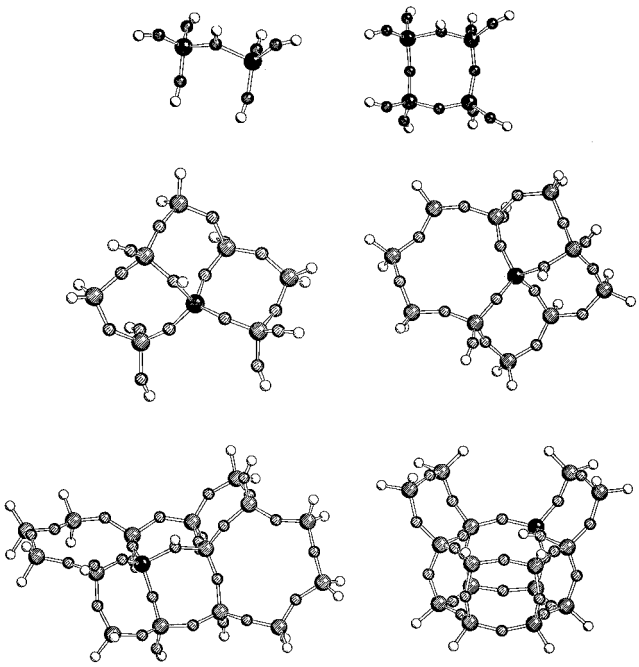

**Figure 9.** Cluster models used for the calculation of the $^1$H NMR chemical shifts of the acidic protons in faujasite. Top left: [T,T] model. Top right: R-4T model. Middle left: FAU-4$^3$ model. Middle right: FAU-6$^1$4$^3$ model. Bottom left: 16T-O1 model. Bottom right: 16T-O3 model. All models have the structure obtained by an embedded cluster optimization using di-tetrahedra models.

membered ring model, [R-4T], into a periodic environment described by the shell model potential. The chemical shifts calculated are the same if the same cluster, e.g. [T,T], is used for the chemical shift calculations, but different clusters, e.g. [T,T] and [R-4T] are employed in the structure optimizations by the combined QM−Pot scheme. This shows that the optimized structures obtained with the two different embedded cluster optimizations are very similar. To obtain converged chemical shifts, it is necessary to use larger clusters than the clusters embedded for the structure optimization. Also, the convergence is different for different oxygen positions. For example in the periodic structure the protons at both the O2 and O3 positions point into a six-membered ring, while in the FAU-6$^1$4$^3$ model this is only the case for the proton at the O2 position. For this reason models even larger than the FAU-6$^1$4$^3$ model were designed which put the proton in the middle of the cluster, with the consequence that different cluster models were used for different positions. One condition was that the different cluster models have the same Si/Al ratio.

The observed sequence of proton shifts for the O1 and O3 position[46] is reproduced only for models containing as many as 16 $TO_4$ tetrahedra. Table 8 shows that the chemical shift for the proton located at the O1 position is already converged for the FAU-4$^3$ model, while for the proton at the O3 position larger clusters are necessary. The different convergence of proton NMR chemical shifts shows that it is not only the local structure which determines the chemical shift. The higher shift of the proton at the O3 position is due to the more dense environment provided by the double six-ring, while the environment for the proton position O1, which points into the large supercage, is less dense.

A relation between the acidity and the chemical shift of a proton was postulated several times. The reasoning was as follows:[47] The deprotonation is the easier the higher the net charge is. From the higher net charge a lower electron density follows. The nucleus is therefore less shielded. Quantum mechanical calculations showed earlier that such a relation does not exist for a broad class of compounds with XOH groups.[5] The reason is that lone electron pairs on O and X−O bonding pairs make nonconstant and nonnegligible contributions to the chemical shift.[5] Only for a limited set of hydroxyl groups could such a relation be verified. Here we deal with one type of surface hydroxyl groups which differ only by their environment in the crystal. Figure 10 shows the plot of the chemical shift of the protons versus the deprotonation energies. There is no general correlation. If, however, only the O(1)H and O(3)H protons are considered, for which observed data exist, a lower deprotonation energy is connected with a larger chemical shift. Although this is the expected relation, Figure 10 shows that it is not generally true.

**TABLE 8: $^1$H NMR Chemical Shifts (ppm) of the Acidic Sites of Faujasite. Calculations Were Carried Out at the Structures Optimized with the Embedded Cluster Method**

| models[a] | O(1)H | O(2)H | O(3)H | O(4)H |
|---|---|---|---|---|
| [T,T]//[T,T] | 3.9 | 4.1 | 3.6 | 4.2 |
| [T,T]//[R-4T] | 3.9 | 4.1 | 3.6 | 4.2 |
| [R-4T]//[R-4T] | 4.0 | 4.1 | 3.8 | 4.2 |
| FAU-4$^3$//[T,T] | 4.3 | | 4.4 | |
| FAU-4$^3$//[R-4T] | 4.3 | | 4.3 | |
| FAU-6$^1$4$^3$//[T,T] | 4.4 | 4.9 | 4.4 | 4.6 |
| 16T//[T,T] | 4.3 | 5.0 | 4.7 | 4.3 |
| obsd[b] | 3.9 | | 4.6 | |

[a] Cluster 1//cluster 2 means that chemical shift calculations are made for cluster 1 at the structure obtained by QM−Pot calculations for the embedded cluster 2. [b] Reference 46.

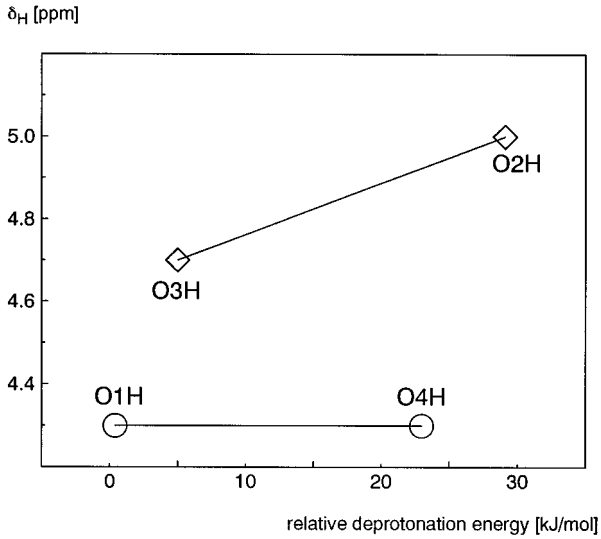


**Figure 10.** Relation between the deprotonation energy and $^1$H NMR chemical shift for the four proton positions in faujasite.

## 5. H-ZSM-5

**5.1. Sites Considered and Models Adopted.** Because of its industrial importance H-ZSM-5 was already the subject of numerous theoretical investigations.[18−22,48−50] The typical building unit of ZSM-5 is a five-membered ring. Two different channels exist built by 10-membered rings, a straight channel and a zigzag channel. The location and characterization of catalytically active sites in ZSM-5 is much more demanding than in faujasite since the monoclinic modification has 24 crystallographically different tetrahedral sites into which aluminum atoms could be substituted and there are 96 different possibilities to form an acid site by attaching the proton to any of the four O atoms surrounding a particular Al site. Schröder et al.[49] performed lattice energy minimizations on all of these substitution products using an empirical shell model potential.

**TABLE 9: Relative Lattice Energies and Deprotonation Energies for the Protonated ZSM-5 Structures Obtained by Shell Model Potential and Embedded Cluster Calculations (kJ/mol)**

| | Al7−O17−Si4 | Al12−O24−Si12 | Al2−O6−Si6 |
|---|---|---|---|
| shell model potential | | | |
| relative energy | 0.0 | 8.4 | 2.1 |
| embedded [T,T] cluster | | | |
| relative energy | 0.0 | 10.6 | 7.1 |
| $\Delta E^{QM-Pot}$ | 1286.0 | 1274.8 | 1278.8 |
| $\Delta E^{QM//QM-Pot}$ | 1363.3 | 1391.1 | 1347.5 |
| $\Delta E^{LR//QM-Pot}$ | −77.3 | −116.3 | −68.7 |
| embedded R-5T cluster | | | |
| relative energy | 0.0 | | 18.4 |
| $\Delta E^{QM-Pot}$ | 1281.6 | | 1267.6 |
| $\Delta E^{QM//QM-Pot}$ | 1312.7 | | 1339.5 |
| $\Delta E^{LR//QM-Pot}$ | −31.1 | | −71.9 |

**TABLE 10: Optimized Structures of H-ZSM-5 (Å, deg)**

| | Al7−O17H−Si4 | | | Al12−O24H−Si12 | | | Al2−O6H−Si6 | | |
|---|---|---|---|---|---|---|---|---|---|
| | embedded cluster | | shell model potential | embedded cluster | | shell model potential | embedded cluster | | shell model potential |
| | [T,T] | R-5T | | [T,T] | shell-4[a] | | [T,T] | R-5T | |
| $r$(Al−O) | 1.901 | 1.912 | 1.923 | 1.880 | 1.885 | 1.895 | 1.909 | 1.911 | 1.921 |
| $r$(Si−O) | 1.700 | 1.698 | 1.691 | 1.688 | 1.683 | 1.686 | 1.693 | 1.702 | 1.693 |
| $r$(Ob−H) | 0.9558 | 0.9564 | 0.9573 | 0.9570 | 0.9566 | 0.9622 | 0.9648 | 0.9586 | 0.9677 |
| $r$(Al−H) | 2.443 | 2.442 | 2.438 | 2.373 | 2.379 | 2.370 | 2.395 | 2.365 | 2.366 |
| ∠(Al−O−Si) | 131.5 | 132.0 | 135.4 | 135.9 | 135.8 | 138.4 | 137.6 | 139.8 | 141.7 |

[a] This model includes four complete coordination shells around the central OH group. Cf. Figure 12 bottom.

For the monoclinic structure studied the Al7−O17(H)−Si16 and Al19−O43(H)−Si4 sites proved most stable. We study here the orthorhombic form which ZSM-5 assumes at high temperatures or at loadings with adsorbates. On the monoclinic−orthorhombic structure transition the two sites found by Schröder et al. collapse into one, Al7−O17(H)−Si4, which we will call a "regular" site. In addition, the Al12−O24(H)−Si12 site is investigated, which has been studied previously by several groups.[18−22] Recently Beck et al.[51] discovered an unexpected peak at 6.9 ppm in the $^1$H MAS NMR spectrum of H-ZSM-5. Combining this with the earlier observation of a broad band at 3250 cm$^{-1}$ in the IR spectrum by Zholobenko et al.[52] leads to the assumption that an intramolecular hydrogen bond could be responsible for both properties.[53] For this reason another position, Al2−O6(H)−Si6, was chosen[53] in which the proton of the acid site can extend a hydrogen bond to an oxygen atom belonging to the same five-membered ring of the zeolite framework.

The structures of these acidic sites were determined by lattice energy minimization using the combined QM−Pot scheme and the shell model potential only. The smallest reasonable model, the di-tetrahedra model, was used for the embedded cluster calculations for all of the sites investigated. The proper description of the hydrogen bond at the Al2−O6−Si6 position requires the use of a five-membered ring as a model. For comparison, a five-membered ring was also chosen as an additional model for the regular site. The start structures and cell parameters for the H-ZSM-5 crystals with Brønsted sites in different positions were determined by lattice energy minimization using the shell model potential.

**5.2. Results.** Table 9 shows the relative lattice energies and the absolute deprotonation energies of the acidic sites. Both the shell model potential calculation alone and the embedded cluster calculations predict the Al7−O17(H)−Si4 site as the most stable one. The choice of the Al12−O24(H)−Si12 site seems to be rather arbitrary. The results of Schröder et al.[49] indicate that there may be many other sites with lower energies.

The deprotonation energies are determined for the embedded di-tetrahedra and five-ring models by the same combined QM−Pot technique as used for faujasite above. The deprotonation energies of the different sites are in a narrow range of 10 kJ/mol. The regular site has the highest deprotonation energy. The differences between the two embedded cluster results for the Al2−O6(H)−Si6 site are larger than the typical error of 5 kJ/mol (section 4.2 and ref 15) since the hydrogen bond is substantially better described by a five-ring model.

Table 10 shows the local structure of the acidic sites. For the cell parameters see Table S2 of the Supporting Information. Figure 12 shows the structure of the active sites using results for the largest clusters studied. Combined QM−Pot calculations predict a smaller bridging Al−O−Si angle than lattice energy minimizations, which use the shell model potential only. As for faujasite, the structure of the active site depends on its location within the framework. Therefore, different properties of the proton arise.

The $^1$H NMR chemical shifts and vibrational OH frequencies were determined using the same techniques as described for faujasite. As already shown for faujasite, the determination of the $^1$H NMR chemical shifts requires larger models than used for structure determination by the combined QM−Pot method. For this reason models with 16 tetrahedral sites were cut out from the embedded [R-5T] cluster equilibrium structure (see Figure 13). Table 11 shows the results. The vibrational frequencies and $^1$H NMR chemical shift of the regular Al7−O17H−Si4 site are in reasonable agreement with the observed values. For the Al2−O6(H)−Si6 site with the "internal H-bond" the predicted vibrational frequency is too high and the predicted $^1$H NMR chemical shift too low. However, the trend compared with the values predicted for the regular site is right. If a H-bond is present, we expect a lower vibrational wavenumber and a larger proton chemical shift. It is known that inclusion of correlation energy is essential to obtain better results for hydrogen-bonded systems. One option with computationally modest demands is the use of a density functional method.[53]

## 6. Discussion

**6.1. Fixed Boundary Atoms and Comparison with Previous Work.** One important feature of our combined QM−Pot scheme is that during structure optimization the forces on the

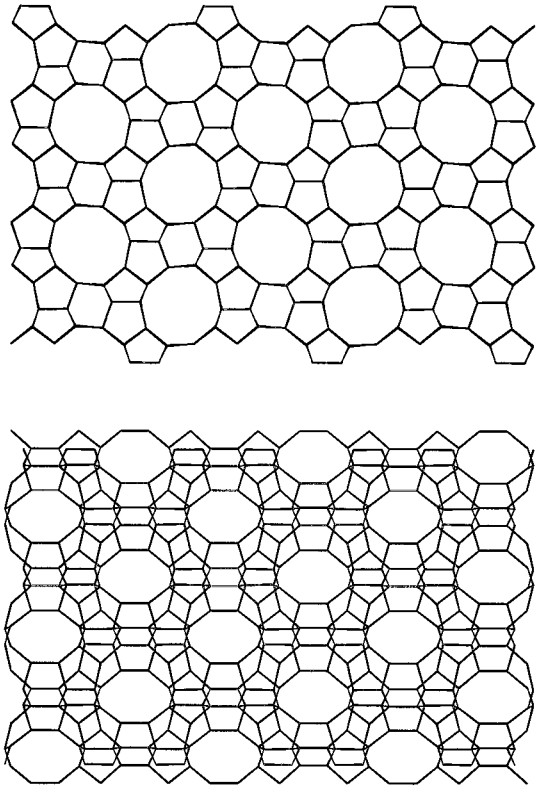

**Figure 11.** ZSM-5 framework. Top: straight channels. Bottom: zigzag channel. For simplicity only the positions of the tetrahedral atoms are shown.

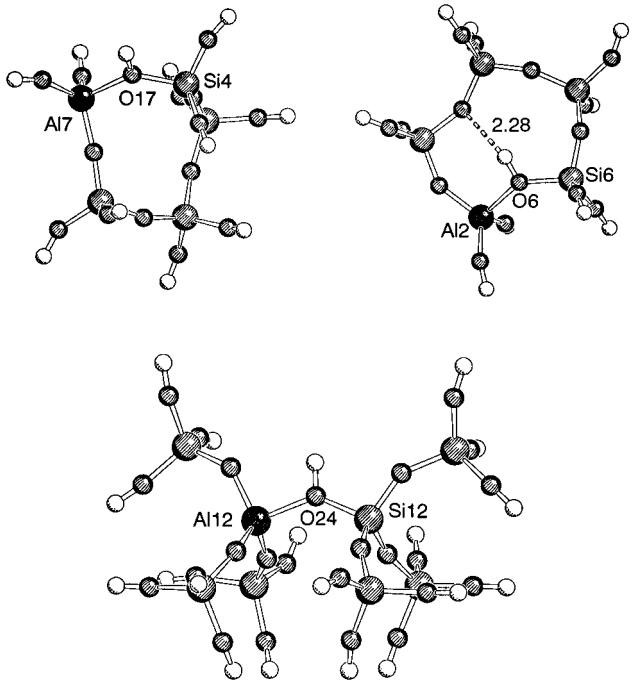


**Figure 12.** Optimized structures of embedded cluster models for Brønsted sites of H-ZSM-5. Top left: Al7−O17−Si4 site ("regular"). Top right: Al2−O6−Si6 site ("H-bond"). Bottom: Al12−O24−Si12 site ("Brand").

atoms of the QM cluster have contributions from atoms of the whole periodic lattice (cf. eq 2). Therefore, we also use the term "mechanical" embedding. An alternative way of imposing constraints to structure optimizations and of making the results framework specific is to fix the boundary atoms of the cluster to positions they have in the periodic lattice and to optimize the positions of the remaining internal atoms only.[18−23] To

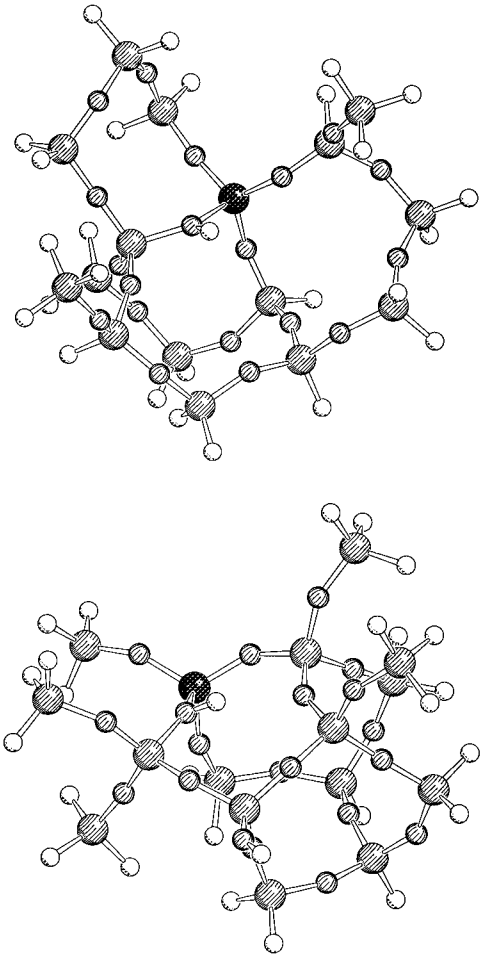

**Figure 13.** Cluster models used for the calculation of the $^1$H NMR chemical shift for the protons in H-ZSM-5. The clusters were cut out from the minimum energy structures. Top: Al7−O17−Si4 site ("regular"). Bottom: Al2−O6−Si6 site ("H-bond").

illustrate this point, we have performed a series of constrained structure optimizations for the Al12−O24(H)−Si12 site. Models with two, three, and four complete shells of Si or O atoms around the central OH group were embedded in the ZSM-5 lattice (shell-2 = [T,T], shell-3 and shell-4 models, cf. Figure 12, bottom). The positions of the terminal hydroxyl or silyl groups were kept fixed at the Cartesian coordinates found by an initial shell model potential calculation of the ZSM-5 lattice including these sites. Table 12 shows the results. Convergence with increasing cluster size is much slower than for the fully relaxed structures obtained by the combined QM−pot method (Table 10). Previous studies used "observed" structures to fix the coordinates of the outer atoms, which average over all Si and Al atoms at a given crystallographic site. Since the average AlO distance is about 0.13 Å longer than the average SiO distance, fixing atoms to average positions may cause artificial strain, especially for clusters in which relaxation is only allowed for a small set of atoms. The structures optimized by Brand et al.[19] show changes as large as 0.2 Å and 5° when comparing the smallest model, 2, with the $8_2$ model (see, for example, the HF/6-31G* results in Table I of ref 19). Similarly, the Si−O−Al angles found for models 2 and 4b of Stave and Nicholas[22] ([T,T] and shell-4 in the language of this study) differ by 10°. The results also very much depend on which X-ray structure data were used, the "Olsen" structure or the "van Koningsveld" structure.[19] The latter seems to yield superior results.

Kyrlidis et al.[21] and Greatbanks et al.[23] add point charges to the Hamiltonian of the cluster to include long-range interactions. The former note that the structure of the Brønsted site remains

**TABLE 11: Calculated and Observed OH Stretching Frequency, $\nu_{OH}$ ($cm^{-1}$), and $^1H$ NMR Chemical Shift, $^1\delta_H$ (ppm), of Different OH Sites in H-ZSM-5**

| | $\nu_{OH}$ | | $^1\delta_H$ NMR | |
|---|---|---|---|---|
| | Al7−O17−Si4 | Al2−O6−Si6 | Al7−O17−Si4 | Al2−O6−Si6 |
| [T,T]//[T,T] | 3594[a] | 3485[a] | 3.72 | 3.28 |
| R-5T//R-5T | 3585[a] | 3532[a] | 3.75 | 4.46 |
| 16T//R-5T | | | 4.41 | 4.71 |
| obsd | 3610[b] | 3250[c] | 4.3[d] | 6.9[d] |
| | | | 4.2[e] | 7.0[e] |

[a] Scaled with 0.89. [b] Reference 43. [c] Reference 52. [d] Reference 51. [e] Reference 54.

**TABLE 12: Local Structures (Å, deg) of the Si12−O24(H)−Al12 Acidic Site of H-ZSM-5 Obtained by Constraint Optimization**

| | this work, T(O)DZP | | | Brand et al.[a] HF/6-31G* | Kyrlidis et al. LDA/ps-Min[b] | Stave and Nicholas LDA/DNP+ |
|---|---|---|---|---|---|---|
| model | [T,T] | shell-3[c] | shell-4[c] | shell-3[c] | pentamer (T5) | shell-4[c,d] |
| $r$(Al−O) | 1.972 | 1.882 | 1.919 | 1.83 | 1.81 | 1.84 |
| $r$(Si−O) | 1.682 | 1.669 | 1.684 | 1.65 | n.r.[e] | 1.66 |
| $r$(O−H) | 0.9541 | 0.9546 | 0.9543 | 0.954 | 1.04 | 0.978 |
| $r$(Al−H) | 2.401 | 2.394 | 2.372 | n.r.[e] | 2.33 | n.r.*e* |
| ∠(Al−O−Si) | 139.3 | 136.4 | 138.8 | 132 | 135 | 135 |

[a] Reference 19. [b] Reference 21, Hellman−Feynman forces only. [c] Shell-*n* denotes models with *n* complete coordination spheres around the central OH group. Cf. Figure 12 bottom for the shell-4 model. [d] Reference 22; only a shell-2 subset of atoms is optimized. [e] Not reported.

practically unchanged in the presence of the Madelung field. The latter report changes of 0.04, 0.015, and 0.005 Å for the Al−O, Si−O, and O−H bond. For comparison, Table 12 also shows the "best" results from previous cluster calculations with fixed boundary atom positions. Comparison is easiest with the results of Brand et al.[19] since they also employed the HF approximation and adopted a similar basis set. The largest deviations from our fully relaxed structure (Table 10: 1.88, 1.68, and 0.957 Å for the Al−O, Si−O, and O−H distances and 136° for the Si−O(H)−Al bond angle) are 0.05 Å for the Al−O distance and 5° for the Al−O(H)−Si angle. Note that the general uncertainty of HF structures is about 0.02 Å and 2−3° and that the OH bonds are systematically too short by 0.012 Å with an uncertainty of about 0.004 Å.[32] Kyrlidis et al.[21] and Stave and Nicholas[22] both use the LDA method, but the former make additional approximations (pseudopotentials, Hellmann−Feynman forces only). The results of Stave and Nicholas[22] are very similar to the present ones, except for the OH bond. It is known that LDA yields too long OH bonds.[4]

We conclude that fixing atoms at the border of the cluster is inferior to our embedded cluster scheme, which relaxes all atoms. If unavoidable, the atoms should be fixed to positions found by a lattice energy minimization instead of using average "observed" positions. Even then, however, the specific differences between Brønsted sites in different crystallographic positions may be lost in such models. An example is the four different OH groups in faujasite. Structures predicted by the combined QM−Pot scheme for the same Brønsted site agree well if clusters of different size are used. In contrast the structures obtained by cluster calculations in which the terminal groups are fixed to positions obtained by lattice energy minimization show larger deviations; especially the Al−$O_b$ distances are too long (Table 4). The characteristic pattern, O3H and O2H longer than O1H and O4H, is the same for the embedded [T,T] and [R-4T] clusters, but the calculations with the fixed terminal hydroxyl groups do not reproduce this sequence (see Figure 14).

Getting converged results proves more difficult for deprotonation energies than for structures. In their first study Brand et al.[18] observed an oscillation of the deprotonation energy with an increasing number of shells of atoms about the central SiO(H)Al bridge. The difference between H-saturated and OH-saturated clusters was as large as 120 kJ/mol, even for models

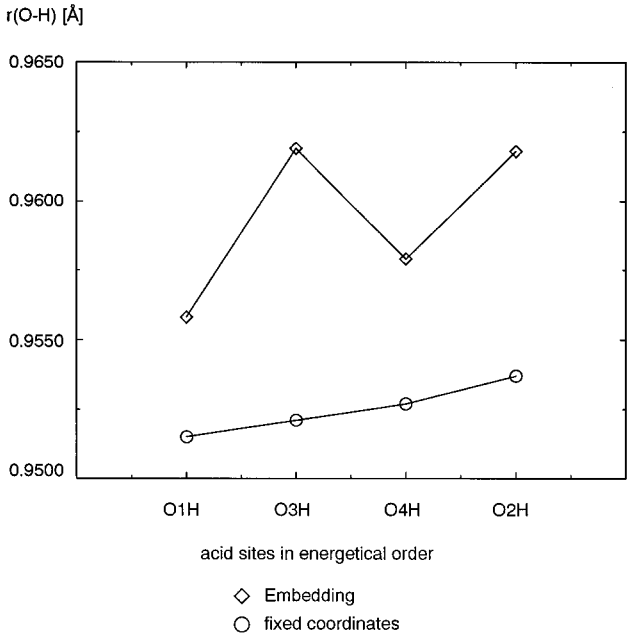


**Figure 14.** OH distances of the four different acidic sites in H-faujasite. Comparison of embedded cluster calculations with calculations using fixed boundary atoms.

with two shells of oxygen atoms and two shells of silicon atoms. In their second study, Brand et al. performed a careful analysis of the dependence on the size and the shape of cluster models.[19] The largest cluster considered had 46 T-sites, and corrections were made for the incorrect O/Si(Al) ratio, which in most models is different from its ideal value of 2. The final extrapolated HF/6-31G* result of 1291 kJ/mol is in very good agreement with our embedded cluster result of 1275 kJ/mol (Table 9). Even the fact that our number is slightly smaller is understandable as we use a richer basis set which describes the anion better than the 6-31G* basis set. Stave and Nicholas[22] calculate for their largest cluster 1336 kJ/mol, a very likely result in view of the OH termination and the neglected long-range corrections. In contrast, the deprotonation energies reported in ref 21 appear to be odd: 1432 kJ/mol for the OH-terminated pentameric cluster and 1654 kJ/mol for the cluster embedded in a Madelung field. The former value is already so large that it is typical of a very weakly acidic terminal SiOH group,[55,56]

**TABLE 13: Acidic Sites of H-Faujasite and H-ZSM-5: Comparison of the OH Frequencies, $\nu_{OH}$ ($cm^{-1}$), $^1H$ NMR Chemical Shifts, $^1\delta_H$ (ppm), Local Structures (Å, deg), and Deprotonation Energies, $\Delta E$ (kJ/mol)**

| | H-faujasite O(1)H | H-ZSM-5 Al7−O17H−Si4 | H-faujasite O(3)H |
|---|---|---|---|
| Si/Al[a] | 47 | 95 | 47 |
| $\nu_{OH}$ | | | |
| predicted[b] | 3596 | 3585 | 3537[c] |
| obsd | 3623[d] | 3610[e] | 3550[d] |
| | 3627[f] | | 3554[f] |
| $^1\delta_H$ | | | |
| predicted | 4.3 | 4.4 | 4.7 |
| obsd[g] | 3.9 | 4.2 | 4.6 |
| $r_{OH}$[h] | 0.9556 | 0.9564 | 0.9606[c] |
| ∠SiO(H)Al | 125.7 | 132.0 | 133.5 |
| Δ(∠SiOAl)[i] | 10.9 | 18.4 | 14.9 |
| $\Delta E_{DP}$ | 1250 | 1286 | 1247 |
| $\Delta E_{DP}^{vertical}$ | 1382 | 1436 | 1397 |
| $\Delta E_{relax}$ | −132 | −150 | −149 |
| $\Delta E_{QM//QM-Pot}$ | 1369 | 1363 | 1344 |
| $\Delta E_{LR//QM-Pot}$ | −119 | −77 | −97 |
| $\Delta E_{DP}^{corr}$+ZPE | 1169 | 1205 | 1166 |

[a] Si/Al ratio used in the calculations. [b] R-4T and R-5T models. QM(C)//QM−Pot(S) results scaled by 0.89, cf. Tables 7 and 11. [c] Average of the R-4T models A and B. [d] Si/Al = 21, ref 43. [e] Reference 52 [f] Si/Al = 5.4, ref 58. [g] Reference 46. [h] R-4T and R-5T results from Tables 4 and 10. [i] Change on deprotonation, ∠SiOAl − ∠SiO(H)Al, cf. Tables 4 and 5.

and the Madelung correction seems to work in the wrong direction. A value of 1654 kJ/mol is clearly outside the expected range of theoretical results and also outside the range of the spectroscopically derived values quoted in Table 14 below. Unfortunately, no investigation is made in ref 21 of the dependence of the Madelung correction on the cluster size or shape.

The present combined QM−Pot scheme appears to be more reliable and stable than approaches using a Madelung field[21] and computationally more efficient than large cluster calculations needed to get nearly converged results.[19]

**6.2. Comparison between Brønsted Sites in H-Faujasite and H-ZSM-5.** In this section comparison is made between three types of sites that are often observed in experiments, the O(1)H and the O(3)H sites in H-faujasite (HF and LF IR bands, respectively) and the "regular" site in ZSM-5 (Al7−O17(H)−Si4). Table 13 shows our predictions for the local structure, the spectroscopic properties, and the acidities of these sites. Comparison is made with the observed data available. The observed wavenumbers of the OH vibration decrease according to the sequence O(1)H-FAU > regular (ZSM-5) > O(3)H-FAU, and the $^1H$ NMR chemical shift increases in the same sequence. These sequences are reproduced by the calculated values. This is a major achievement of computational techniques in zeolite chemistry since it means that the relative positions of the OH infrared band and the $^1H$ NMR signal of different zeolitic Brønsted sites can be reliably predicted. Also in absolute terms, there is good agreement between predicted and observed values. The deviations are below 30 $cm^{-1}$ and 0.4 ppm for the OH frequency and the $^1H$ NMR chemical shift, respectively.

The OH bond distances and Si−O−Al bond angles are also significantly different for different crystallographic positions and different framework types. With respect to the acidic reactivity of Brønsted sites, there is also interest in the structure relaxation accompanying deprotonation of the active site. Table 13 shows the change of the Si−O−Al bond angle on deprotonation. The largest change is observed for the "regular" Brønsted site in ZSM-5.

The calculated deprotonation energies for the O(1)H and the O(3) H sites of H-faujasite differ only by 2.9 kJ/mol. The calculated deprotonation energies for H-faujasite are lower than that of the "regular" acidic site in H-ZSM-5. There are several ways of analyzing the acidity differences between different sites and frameworks. First we can decompose the energy of deprotonation into a "vertical" energy defined as

$$\Delta E_{DP}^{vertical} = E(ZO^-//ZOH) - E(ZOH//ZOH)$$

and a relaxation energy defined as

$$\Delta E_{relax} = E(ZO^-//ZO^-) - E(ZO^-//ZOH)$$

with

$$\Delta E_{DP} = \Delta E_{DP}^{vertical} + \Delta E_{relax}$$

Table 13 shows the data. The relaxation energies for the regular site in H-ZSM-5 and for the O(3)H site (LF band) in faujasite are larger than that for the O(1)H site in faujasite. The final acidity difference between the O(1)H site in faujasite and the regular site in H-ZSM-5 is a superposition of the structure relaxation, which is more favorable for the H-ZSM-5 site, and the crystal potential term discussed below, which is more favorable for H-faujasite. The crystal potential term appears to be the decisive contribution.

Second, the deprotonation energy of the embedded clusters can be separated into two contributions, the quantum mechanical energy of the embedded cluster, $\Delta E_{QM//QM-Pot}$, and the influence of the electrostatic long-range contribution of the framework, $\Delta E_{LR//QM-Pot}$ (cf. eq 9). The deprotonation energy of the quantum mechanical part is 1369 kJ/mol for the O(1)H site in faujasite and 1363 kJ/mol for the regular site in H-ZSM-5. The difference between H-Y and H-ZSM-5 in constraining the relaxation is small, about 6 kJ/mol. However, the long-range influence of the framework is much more important and amounts to −119 and −77 kJ/mol for H-faujasite and H-ZSM-5, respectively. The difference is 42 kJ/mol. When a larger cluster, a tri-tetrahedra model (Figure 5), is embedded, these long-range contributions become smaller, −102 and −70 kJ/mol for H-faujasite and H-ZSM-5, respectively, and also their difference decreases. However, the quantum mechanical cluster energies also change; for the tri-tetrahedra models they are 1354 and 1358 kJ/mol, respectively, so that the total QM−Pot results, 1252 and 1288 kJ/mol, respectively, agree within 2 kJ/mol with the values in Table 13.

To compare the final deprotonation energies (QM−Pot results) with values derived from experiments, the systematic deviations due to the error of the Hartree−Fock approximation and the basis set truncation must be taken into account. These corrections are −46 kJ/mol for the T(O)DZP basis set used.[57] Nuclear motion corrections due to the loss of three vibrational degrees of freedom of the acidic proton are fairly constant over a wide range of XOH systems. Both ab initio calculations on small free space optimized models,[5] e.g. $H_3SiOHAl(OH)_3$, and shell model potential calculations on periodic zeolite structures performed within this study for the O(1)H site of H-faujasite yield zero-point vibrational corrections of −32 kJ/mol. Thermal corrections are 1 order of magnitude smaller, and the total nuclear motion corrections are about −35 kJ/mol. The uncertainty connected with these corrections is about ±10 kJ/mol. Hence, our final estimates for the O(1)H and O(3)H sites of faujasite are 1169 and 1166 kJ/mol, respectively, while for the regular site in H-ZSM-5 1205 kJ/mol is predicted. This means that H-ZSM-5 is less acidic than H-faujasite, provided that both

**TABLE 14: Heat of Deprotonation (Proton Affinity, kJ/mol) Predicted by ab Initio Calculations and Inferred from OH Frequency Shifts**

| | H-ZSM-5 | | H-faujasite | | |
|---|---|---|---|---|---|
| | Si/Al | result | Si/Al | result | ref |
| predicted | 95 | 1205 | 47 | 1166−1169 | this work |
| derived from $\delta\nu_{OH}$ | (50)[a] | 1170[b] | (2.5)[a] | 1190[b] | 63 |
| | | | (2.5)[a] | 1200 ± 25 | 56 |
| | | | 2.7 | 1161−1177 | 58 |
| | 16 | 1147−1154 | 5.4 | 1142 | 58 |
| | 47 | 1178−1236 | | | 59 |

[a] Si/Al ratio not explicitly given in the paper quoted. Standard values specified. [b] Numbers taken fom the points in Figure 3 of ref 63.

catalysts have large Si/Al ratios as assumed in the calculations. Calculations with the shell model potential have shown that the assumption of different Si/Al ratios in our calculations (47 for H-faujasite and 95 for H-ZSM-5) does not have any noticeable effect. Moreover, in experiments no change with increasing Si/Al ratio is observed beyond Si/Al of about 15.

For surface hydroxyls experimental values of heats of deprotonation are not directly accessible, but inferences can be made from OH frequency shifts on complex formation with a series of base molecules. Deprotonation energies are derived by comparing the frequency shifts observed for OH acids in the gas phase with those of surface hydroxyls using the same set of base molecules. Table 14 shows the results available. Among the catalysts studied experimentally H-ZSM-5 has the largest Si/Al ratio and is most suited for a direct comparison. The results from different authors derived using different base molecules and different reference acids scatter over a range of almost 90 kJ/mol. The predicted value, 1205 kJ/mol, falls into this range. Makarova et al.[58] adsorb CO and use the relation proposed in ref 56 to derive the deprotonation energy relative to a value of 1390 kJ/mol for terminal SiOH groups. Datka et al.[59] adsorb several molecules (*n*-hexane, benzene, toluene, *p*-xylene, and ethene) and use phenol, acetic acid, benzoic acid, chloroacetic acid, and trifluoroacetic acid as reference acids. The results obtained for H-ZSM-5 vary between 1178 and 1236 kJ/mol. A broad OH band typical of H-bonded systems is observed on adsorption of the above base molecules. This band shows some structure, and Datka et al. decomposed it into five subbands, from which they derived five different acidity values: 1179, 1210, 1226, 1260, and 1333 kJ/mol.[60] They tentatively ascribed these values to SiO(H)Al groups of different crystallographic sites in H-ZSM-5. From the present study we learn that acidity differences between different sites in H-ZSM-5, e.g. between the "regular" (Al7−O17H−Si4) and the "Brand" (Al12−O24H−Si12) or the "H-bond" site (Al2−O6H−Si6) are small, not exceeding 15 kJ/mol (Table 9). Hence, the variation between 1179, 1210, and 1226 kJ/mol may be explained by different crystallographic sites, while it seems to be unlikely that the values 1260 and 1333 are due to special positions in the ZSM-5 framework. Other candidates are defect sites. The value of 1333 kJ/mol even comes close to the result of 1390 ± 25 kJ/mol reported for terminal hydroxyls.[56]

Our prediction for catalysts with a faujasite-type framework is made for a highly siliceous catalyst with Si/Al = 47, while results derived from the OH frequency shifts are available for H-Y zeolites, which have a typical Si/Al ratio as low as 2.5. Hence, it is not a contradiction that the OH frequency shifts indicate that H-Y is less acidic (has a higher heat of deprotonation) than H-ZSM-5, while we predict that for a high Si/Al ratio bridging hydroxyls in the faujasite framework are more acidic than in the ZSM-5 framework. It is known from experiments that increasing the Si/Al ratio also increases the acidity. For example, Makarova et al. studied a partially dealuminated (ultrastable) zeolite Y with a framework Si/Al ratio of 5.4. From the OH frequency shift of the HF band on CO adsorption they derive a heat of adsorption of 1142 kJ/mol, slightly less than the 1147−1154 kJ/mol derived for H-ZSM-5.[58] It is an advantage of computational techniques that parameters such as framework structure and Si/Al ratio can be independently varied. Indeed, in an accompanying theoretical study which uses also the embedded cluster methodology we show that the deprotonation energy of bridging SiO(H)Al groups in H-Y with Si/Al = 3.0 is 20−30 kJ/mol higher than in H-faujasite with Si/Al = 47.[61]

We also note that different measures of acidity may yield different relative acidities. A popular measure of acidity is the heat of $NH_3$ adsorption obtained by temperature-programmed desorption or microcalorimetry. A parallel study[62] applies the combined QM−Pot scheme to $NH_3$ adsorption on Brønsted sites in faujasite, ZSM-5, chabazite, and mordenite. Comparison is made with the heat of deprotonation. While there are some changes of the relative acidities when the two acidity scales are compared, this does not affect the relative acidities of H-faujasite and H-ZSM-5. The heat of $NH_3$ adsorption is smaller (in absolute terms) for H-ZSM-5 than for H-faujasite (large Si/Al ratio), which confirms that H-ZSM-5 is less acidic than H-faujasite provided that both catalysts have large Si/Al ratios.

## 7. Conclusions

A combined quantum mechanics/interatomic potential function approach is presented which describes the active site by the ab initio Hartree−Fock method and the periodic zeolite framework by an ab initio-parametrized shell model potential. Boundary effects are minimized by a special treatment of the link atoms (hydrogen atoms introduced to terminate the dangling bonds of the quantum mechanical part) and by a parametrization of the potential which is based on the same type of ab initio data as used for the quantum mechanical cluster. Embedded cluster calculations using this method can differentiate between Brønsted sites in different crystallographic positions of a given framework and between Brønsted sites in different frameworks. This is a significant advancement compared to previous cluster calculations.

Several "internal" tests of the methods are made, mainly by observing the stability of the results with increasing the size of the quantum mechanical cluster. The embedded cluster results converge much faster than free space cluster results or cluster results obtained for fixed positions of the outer atoms. The absolute error of the total energy is below 10 kJ/mol. Relative energies may be even more accurate.

The method is primarily used to predict the structures of catalysts protonated at different sites. The structure found is then used to predict OH vibrational frequencies. Best results are obtained if force constants are used calculated for the quantum mechanical energy surface of the cluster alone, but taken at the equilibrium structure found by the combined QM−Pot method. These structures are also used to calculate $^1$H NMR chemical shifts by the GIAO coupled perturbed Hartree−Fock method. For these calculations—which do not include the crystal potential—much larger clusters containing as many as 16 $TO_2$ units have to be used to get converged results.

When the combined QM−Pot scheme is applied to deprotonation reactions, embedded cluster calculations have to be made for both the parent system and the deprotonated system. In the latter case a negative charge is created in every unit cell.

To obtain nonsingular energies for such systems, a positive uniform background charge is added to every unit cell and the interaction between defects in different unit cells is eliminated by adding a classical compensation term. It is shown that for the large unit cell of zeolites this procedure leads to errors below 2 kJ/mol.

The total deprotonation energy—a measure of acidity—obtained by the combined QM−Pot scheme can be decomposed into the quantum mechanical contribution for the cluster itself and into the long-range contribution. The former reflects the structural constraints imposed on the active site by the framework and the latter the influence of the crystal potential. With increasing cluster size the long-range correction is found to decrease slowly, while the total QM−Pot energy stays remarkably stable within a few kJ/mol.

The method is applied to the H-faujasite (Si/Al = 47) and to H-ZSM-5 (Si/Al = 95). For faujasite, protonation of all four crystallographically different oxygen positons is considered. In agreement with experiment, protonation on O(1) and O(3) is found to be preferred. For the orthorhombic form of H-ZSM-5 the "regular" site, Al7−O17(H)−Si4, is selected, which proved most stable in previous shell model potential simulations. Protonation at Al12−O24−Si12 located at the channel intersection as assumed by Brand et al.[19] is also considered and found less stable. For protonation at the Al2−O6−Si6 site the formation of an internal H-bond inside a five-membered silicate ring seems to be possible.

For the O(1)H and O(3)H sites of faujasite and the "regular" acidic site in ZSM-5 the wavenumbers of the OH vibrational band are predicted to decrease according to O(1)H-FAU > regular (ZSM-5) > O(3)H-FAU, and the $^1$H NMR chemical shift to increase in the same sequence. Hence, the combined QM−Pot method is capable of reliably predicting the relative positions of the OH infrared band and the $^1$H NMR signal of different zeolitic Brønsted sites. For similarly large Si/Al ratios (95 and 47), H-ZSM-5 is predicted to be less acidic than H-faujasite. The deprotonation energies are 1205 and 1169 kJ/mol, respectively. The reason is the difference in crystal potentials. Generally, for a given Si/Al ratio, acidity differences between different sites and frameworks are due to differences of both the local structures (including the structure relaxation) and the crystal potentials. Simple correlations with the T−O−T bond angle or the $^1$H NMR chemical shift do not exist. Deprotonation energies inferred from OH frequency shifts scatter over 90 kJ/mol and depend on the base molecule adsorbed and the reference acid. That these values indicate a stronger acidity for H-ZSM-5 compared to H-Y is ascribed to the much lower Si/Al ratio of H-Y (2.5).

**Acknowledgment.** We thank Dr. K.-P. Schröder for valuable discussions and providing unpublished results, as well as Prof. R. Ahlrichs (Karlsruhe) and Dr. J. Gale (London) for making available recent versions of the TURBOMOLE and GULP codes, respectively. M.B. thanks the "Alexander von Humboldt−Stiftung" for a research fellowship. This work has been supported by the "Deutsche Forschungsgemeinschaft" and by the "Fonds der Chemischen Industrie".

## Appendix

The first and second strain derivatives of the correction term $E_{BC}$ (eq 10) were derived by following the procedure outlined by Catlow and Mackrodt[64] for the strain derivatives of the shell model potential energy. The bulk strains $\{\epsilon_k\}$, $k = 1, ..., 6$, used below form the components of the symmetric strain tensor as described in ref 64. At zero strain we get

$$\left.\frac{\partial E_{BC}}{\partial \epsilon_k}\right|_V = -\frac{2}{3}E_{BC} \quad \text{for} \quad k = 1, 2, 3 \tag{A1}$$

$$= 0 \quad \text{for} \quad k = 4, 5, 6$$

$$\left.\frac{\partial^2 E_{BC}}{\partial \epsilon_k^2}\right|_V = \frac{10}{9}E_{BC} \quad \text{for} \quad k = 1, 2, 3 \tag{A2}$$

$$= \frac{1}{3}E_{BC} \quad \text{for} \quad k = 4, 5, 6$$

$$\left.\frac{\partial^2 E_{BC}}{\partial \epsilon_k \partial \epsilon_l}\right|_V = \frac{4}{9}E_{BC} \quad \text{for} \quad \begin{cases} k = 1, 1, 2 \\ l = 2, 3, 3 \end{cases} \tag{A3}$$

$$= 0 \qquad \text{for} \quad \begin{cases} k = 1, 1, 1, 2, 2, 2, 3, 3, 3, 4, 4, 5 \\ l = 4, 5, 6, 4, 5, 6, 4, 5, 6, 5, 6, 6 \end{cases}$$

In the derivation of the above equations notice was made of the fact that the Ewald screening parameter $\eta$ depends on the number of core and shell species $N$ and the volume per unit cell:[65]

$$\eta = \left(\frac{N\pi^3}{V^2}\right)^{1/6} \tag{A4}$$

**Supporting Information Available:** Lattice constants of all protonated and deprotonated faujasite and ZSM-5 structures studied as obtained by shell model lattice energy minimization (2 pages). Ordering information is given on any current masthead page.

## References and Notes

(1) Maxwell, I. E.; Stork, W. H. J. In *Introduction to Zeolite Science and Practice*; Studies in Surface Science and Catalysis, Vol. 58; van Bekkum, H., Flanigan, E. M., Jansen, J. C., Eds.; Elsevier: Amsterdam, 1991; p 571.
(2) Farneth, W. E.; Gorte, R. J. *Chem. Rev.* **1995**, *95*, 615.
(3) Bartmess, J. E.; McIver, R. T., Jr. In *Gas Phase Ion Chemistry*; Bowers, M. T., Ed.; Academic Press: New York, 1979; Vol. 2, p 87.
(4) Sauer, J.; Ugliengo, P.; Garrone, E.; Saunders, V. R. *Chem. Rev.* **1994**, *94*, 2095.
(5) van Santen, R. A.; Kramer, G. J. *Chem. Rev.* **1995**, *95*, 637.
(6) Fleischer, U.; Kutzelnigg, W.; Bleiber, A.; Sauer, J. *J. Am. Chem. Soc.* **1993**, *115*, 7833.
(7) White, J. C.; Hess, A. C. *J. Phys. Chem.* **1993**, *97*, 6398.
(8) White, J. C.; Hess, A. C. *J. Phys. Chem.* **1993**, *97*, 8703.
(9) Anchell, J. L.; White, J. L.; Thompson, M. R.; Hess, A. C. *J. Phys. Chem.* **1994**, *98*, 4463.
(10) Nicholas, J. B.; Hess, A. C. *J. Am. Chem. Soc.* **1994**, *116*, 5428.
(11) Dovesi, R.; Roetti, C.; Freyria-Fava, C.; Apra, E.; Saunders, V. R.; Harrison, N. M. *Phil. Trans. R. Soc. London A* **1992**, *341*, 203.
(12) Shah, R.; Gale, J. D.; Payne, M. C. *Science* **1996**, *271*, 1395.
(13) Nusterer, E.; Blöchl, P. E.; Schwarz, K. *Chem. Phys. Lett.* **1996**, *253*, 448.
(14) Haase, F.; Sauer, J.; Hutter, J. *Chem. Phys. Lett.* **1997**, *266*, 397.
(15) Eichler, U.; Kölmel, C. M.; Sauer, J. *J. Comput. Chem.* **1997**, *18*, 463.
(16) Maseras, F.; Morokuma, K. *J. Comput. Chem.* **1995**, *16*, 1170.
(17) Bakowies, D.; Thiel, W. *J. Phys. Chem.* **1996**, *100*, 10580.
(18) Brand, H. V.; Curtiss, L. A.; Iton, L. E. *J. Phys. Chem.* **1992**, *96*, 7725.
(19) Brand, H. V.; Curtiss, L. A.; Iton, L. E. *J. Phys. Chem.* **1993**, *97*, 12773.
(20) Cook, S. J.; Chakraborty, A. K.; Bell, A. T.; Theodorou, D. N. *J. Phys. Chem.* **1993**, *97*, 6679.
(21) Kyrlidis, A.; Cook, S. J.; Chakraborty, A. K.; Bell, A. T.; Theodorou, D. N. *J. Phys. Chem.* **1995**, *99*, 1505.
(22) Stave, M. S.; Nicholas, J. B. *J. Phys. Chem.* **1995**, *99*, 15046.

(23) Greatbanks, S. P.; Hillier, I. H.; Burton, N. A.; Sherwood, P. *J. Chem. Phys.* **1996**, *105*, 3770.
(24) Sauer, J. *J. Mol. Catal.* **1989**, *54*, 312.
(25) Sauer, J. *Chem. Rev.* **1989**, *89*, 199.
(26) Eichler, U. Ph.D. Thesis, Humboldt-Universität zu Berlin, 1997.
(27) Schröder, K.-P.; Sauer, J. *J. Phys. Chem.* **1996**, *100*, 11043.
(28) Ahlrichs, R.; Bär, M.; Häser, M.; Horn, H.; Kölmel, C. M. *Chem. Phys. Lett.* **1989**, *162*, 165; *Program TURBOMOLE*. TURBOMOLE is commercially available from BIOSYM/MSI: San Diego, CA.
(29) Leslie, M.; Gillan, M. J. *J. Phys. C: Solid State Phys.* **1985**, *18*, 973.
(30) Fuchs, K. *Proc. R. Soc. London A* **1935**, *151*, 585.
(31) Gale, J. D. *J. Chem. Soc., Faraday Trans.* **1997**, *93*, 629.
(32) Sauer, J.; Kölmel, C. M.; Hill, J.-R.; Ahlrichs, R. *Chem. Phys. Lett.* **1989**, *164*, 193.
(33) Huzinaga, S. *Approximate Atomic Wavefunctions*; University of Alberta: Edmonton, 1971; Vols. I, II.
(34) Huzinaga, S. *J. Chem. Phys.* **1965**, *42*, 1293.
(35) Hill, J.-R.; Sauer, J. *J. Phys. Chem.* **1994**, *98*, 1238.
(36) Pulay, P. In *Modern Theoretical Chemistry*; Schaefer, H. F., III, Ed.; Plenum Press: New York, 1977; Vol. 4, p 153.
(37) Dios, A. C. de; Pearson, J. G.; Oldfield, E. *Science* **1993**, *260*,-1491.
(38) Häser, M.; Ahlrichs, R.; Baron, H. P.; Weis, P.; Horn, H. *Theor. Chim. Acta* **1992**, *83*, 455.
(39) Schäfer, A.; Horn, H.; Ahlrichs, R. *J. Chem. Phys.* **1992**, *97*, 2571.
(40) Haase, F.; Sauer, J. *J. Am. Chem. Soc.* **1995**, *117*, 3780.
(41) Chauvel, J. P., Jr.; True, N. S. *Chem. Phys.* **1985**, *95*, 435.
(42) Czjzek, M.; Jobic, H.; Fitch, A. N.; Vogt, T. *J. Phys. Chem.* **1992**, *96*, 1536.
(43) Anderson, M. W.; Klinowski, J. *Zeolites* **1986**, *6*, 455.
(44) Schröder, K.-P.; Sauer, J.; Leslie, M.; Catlow, C. R. A.; Thomas, J. M. *Chem. Phys. Lett.* **1992**, *188*, 320.
(45) Brugmans, M. J. P.; Kleyn, A. W.; Lagendijk, A.; Jacobs, W. P. J. H.; van Santen, R. A. *Chem. Phys. Lett.* **1994**, *217*, 117.
(46) Hunger, M.; Horvath, T.; Engelhardt, G.; Karge, H. G. In *Catalysis by Microporous Materials*; Studies in Surface Science and Catalysis, Vol. 94; Beyer, H. K., Karge, H. G., Kiricsi, I., Nagy, J. B., Eds.; Elsevier: Amsterdam, 1995; p 756.
(47) Hunger, M.; Pfeifer, H. In *Innovation in Zeolite Materials Science*; Studies in Surface Science and Catalysis, Vol. 37; Jacobs, P. A., Jaeger, N. I., Kubelkova, L., Wichterlova, B., Eds.; Elsevier: Amsterdam, 1991; p 453.
(48) Alvarado-Swaisgood, A. E.; Barr, M. K.; Hay, P. J.; Redondo, A. *J. Phys. Chem.* **1991**, *95*, 10031.
(49) Schröder, K.-P.; Sauer, J.; Leslie, M.; Catlow, C. R. A. *Zeolites* **1992**, *12*, 20.
(50) Redondo, A.; Hay, P. J. *J. Phys. Chem.* **1993**, *97*, 11754.
(51) Beck, L. W.; White, J. L.; Haw, J. F. *J. Am. Chem. Soc.* **1994**, *116*, 9657.
(52) Zholobenko, V. L.; Kustov, L. M.; Borovkov, V. Yu.; Kazansky, V. B. *Zeolites* **1988**, *8*, 175.
(53) Sierka, M.; Sauer, J. *Faraday Discuss.*, in press.
(54) Brunner, E.; Beck, K.; Koch, M.; Heeribout, L.; Karge, H. G. *Microporous Mater.* **1995**, *3*, 395.
(55) Sauer, J.; Hill, J.-R. *Chem. Phys. Lett.* **1994**, *218*, 333
(56) Paukshtis E. A.; Yurchenko, E. N. *Usp. Khim.* **1983**, *52*, 426.
(57) Sauer, J. In *Molecular Modelling of Structure and Reactivity in Zeolites*; Catlow, C. R. A., Ed.; Academic Press: London, 1992; p 183.
(58) Makarova, M. A.; Al-Ghefaili, K. M.; Dwyer, J. *J. Chem. Soc., Faraday Trans.* **1994**, *90*, 383.
(59) Datka, J.; Boczar, M.; Rymarowicz, P. *J. Catal.* **1988**, *114*, 368.
(60) Datka, J.; Boczar, M.; Gill, B. *Langmuir* **1993**, *9*, 2496.
(61) Sierka, M.; Datka, J.; Sauer, J. In preparation.
(62) Brändle, M.; Sauer, J. In preparation.
(63) Mastikhin, V. M.; Mudrakowsky, I. L.; Nosov, A. V. *Bruker Rep.* **1989**, *2*, 18.
(64) Catlow, C. R. A.; Mackrodt, W. C. *Computer Simulation of Solids*; Lecture Notes in Physics, Vol. 166; Springer: Berlin, 1982; p 3.
(65) Jackson, R. A.; Catlow, C. R. A. *Mol. Simul.* **1988**, *1*, 207.